

**UCSF**

**UC San Francisco Electronic Theses and Dissertations**

**Title**

Reviving *Stentor coeruleus* as a Modern Model for Morphogenesis: RNA interference reveals Mob1 as an asymmetrically localized polarity protein.

**Permalink**

<https://escholarship.org/uc/item/6tb3c3h1>

**Author**

Slabodnick, Mark Maddock

**Publication Date**

2014

Peer reviewed|Thesis/dissertation

Reviving *Stentor coeruleus* as a Modern Model  
for Morphogenesis: RNA interference reveals Mob1 as an  
asymmetrically localized polarity protein.

by

Mark M. Slabodnick

DISSERTATION

Submitted in partial satisfaction of the requirements for the degree of

DOCTOR OF PHILOSOPHY

in

CELL BIOLOGY

in the

GRADUATE DIVISION



## Dedications and Acknowledgements

I will start by saying that my thesis project was certainly a unique one. I will never forget the experiences I gathered during my graduate career and time in the Marshall lab, and I will always look back on this time fondly. Here I wish to recognize the many people who have contributed to my success as well as those who have kept and continue to keep me sane. But before I begin I first wish to dedicate my work to my family.

I was fortunate to have a great group of classmates to share in my time at UCSF. The Tetrad program does a wonderful job of bringing together groups of people with rather diverse interests and experiences. I learned a good deal through my interactions with all of them over the years and I hope they all know that it has meant a lot to get to know them and call them friends. Whether we were studying, relaxing, playing indoor soccer, board games, camping, skiing, or working – I was always happy to be around them. Likewise, the Marshall lab also provided a source of friendship. To keep from rambling too much, I will simply thank everyone for their constant support and interest and hope they know that I will miss working with all of them. I will especially miss talking with Hiro, Mark, Kim, Susanne, and walks to get coffee with Prachee (I will also dearly miss Philz coffee). Also, to what is commonly referred to as “Team Stentor” in the lab, I must also thank Sarah, Pranidhi, and Tatyana for having the courage to work with *Stentor*, it has been great to work so closely with you all and share my excitement for the system that I have worked so hard on these past few years. I hope we can keep building on the *Stentor* community as we all move forward.

I must also mention all of the family that has contributed to my success over the years. I am lucky to have grown up with two brothers, five step-siblings, four cousins, loving aunts and uncles, supportive grandparents, and my parents. I have also gained more family than I can count through marriage. Their support has meant a lot over the years. I would like to give special acknowledgements to my aunt Christie, who has always been supportive of my education and I cannot thank her enough for everything she has done. To my surrogate parents, the Irwins, whose house I basically grew up in, I want to thank them for their endless support and encouragement. They have influenced my life as much as my direct family and I appreciate all of it. To their son Dan, who I consider a brother, his friendship growing up has shaped my life and without it I am not sure I would be where I am today. And I would like to thank my two brothers, Adam and Noah, for all of their love and support. Despite being spread across the country we remain close and I hope they know how much their friendship means to me.

My mother and father were always more than supportive. It was from them that I gained my interest in science, with trips to the science museum where they got me my first microscope. In the fourth grade they let me go to Space Camp, where my love of science and exploration grew even more. All of this led me to Ohio State where I started my career in research and met Harold Fisk, who as a new professor at the university took a chance on hiring me as an undergrad and to whom I am eternally grateful. His continued support has certainly allowed me to succeed and, I am sure, helped get me to UCSF and beyond.

There are two people that I need to thank who unfortunately passed away before I could complete my PhD. My grandfather, William Slabodnick, and his sister, Norma,

both wanted nothing more than to see me succeed in life and I know would be extremely proud. I especially want to dedicate my work to the two of them as I am thankful for their support throughout my life and miss them both dearly.

Finally, I would like to thank my wife, Liz, for being by my side for the past 11 years. I could not have asked for a better partner, and today we celebrated six years of marriage and I look forward to many more. She has been instrumental in my life, joining me in a move across the country just days after our wedding to drive to San Francisco for graduate school. And now, as we pack for yet another move across country to North Carolina I am glad she will be with me to share in the adventure. Her love and support mean so much to me and she has kept me sane through everything.

## Abstract

Over the last few decades scientists have often turned to one of a handful of well-established model systems in order to address a number of questions about how all of biology functions. This is absolutely useful and at the time that many of these systems were adopted the state of the art technologies were much more limited, which made it much more efficient to focus on just a few organisms to set the scientific standards. However, recently there have been many advances in technology that have allowed for the relatively quick development of new and interesting model organisms. This should allow scientists to tailor what we are working on with the types of questions we want to address without being limited to the handful of established models. The questions I seek to address are those related to morphogenesis and pattern formation, which are vital processes in any organism whether unicellular or multicellular. But in contrast to the developmental biology of plants and animals, the principles of morphogenesis and pattern formation in single cells remain largely unknown. Although all cells develop patterns, they are most obvious in ciliates; hence I have turned to a classical unicellular model system, the giant Heterotrich ciliate *Stentor coeruleus*. Here I show that the RNA interference (RNAi) machinery is conserved in *Stentor*. Using RNAi, I identified the kinase co-activator Mob1 – with conserved functions in cell division and morphogenesis from plants to humans – as an asymmetrically localized patterning protein required for global patterning during development and regeneration in *Stentor*. During this process I worked in collaboration to sequence and assemble *Stentor's* macronuclear genome. There is almost no information on Heterotrich genomes and no estimates for gene copy number in *Stentor*. Using digital droplet PCR, I was able to

determine the average contig copy number in *Stentor* for a handful of loci including the small subunit rDNA gene. Finally, the *Stentor* genus is amazingly diverse. Different species can vary in size, shape, color, and some even contain algal endosymbionts. I identified sources of five species of wild *Stentor* near Woods Hole Marine Biological Laboratory and have also included methods and descriptions of these species. I think there is great potential for tapping natural diversity within the *Stentor* genus to discover new and interesting biology. My work reopens the door for *Stentor* as a model regeneration system with potential for many other areas of study.



## Table of Contents

Chapter 1: Introduction to <i>Stentor coeruleus</i> .....	1
Chapter 2: RNA Interference in <i>Stentor coeruleus</i> .....	14
Chapter 3: Mob1 acts as a global patterning protein in <i>Stentor coeruleus</i> .....	27
Chapter 4: Extent of macronuclear amplification .....	55
Chapter 5: Isolation of five <i>Stentor</i> species from two ponds near Woods Hole Marine Biological Laboratory .....	63
Chapter 6: Materials and Methods .....	73
Chapter 7: References .....	84
Appendix: <i>Stentor</i> Quick Guide .....	90

## List of Tables

Table 1	List of homologs of RNAi machinery found in the <i>S. coeruleus</i> genome.....	16
Table 2	Gene IDs for RNAi machinery used in phylogenetic analysis of Sciwi proteins.....	18
Table 3	Details about RNAi vectors used .....	75
Table 4	Primers used for cloning .....	78

## List of Figures and Illustrations

Figure 1	The Anatomy of <i>Stentor coeruleus</i> .....	2
Figure 2	<i>Stentor</i> is an efficient filter feeder and its prey may be used as a vector.....	4
Figure 3	Stentorin secretion and autofluorescence .....	7
Figure 4	Regeneration of proportionate structures in <i>S. coeruleus</i> .....	9
Figure 5	Phylogenetic tree of <i>S. coeruleus</i> Sciwi proteins .....	15
Figure 6	Cartoon alignment of “DDH” motif in <i>S. coeruleus</i> PIWI-like proteins.....	19
Figure 7	$\beta$ -tubulin(RNAi) results in aberrant cell morphologies. ....	21
Figure 8	RNAi knockdown of $\alpha$ - or $\beta$ -tubulin yields similar morphological defects.....	23
Figure 9	Control RNAi cells have normal morphologies .....	25
Figure 10	Conservation of Mob1 and its localization in <i>Stentor</i> .....	28
Figure 11	Antibody against <i>S. coeruleus</i> Mob1 specifically recognizes its target.....	30
Figure 12	Mob1 localizes to the presumptive posterior during cell division.....	32
Figure 13	Sequence alignment of <i>Stentor</i> Mob1 genes .....	35
Figure 14	Mob1(RNAi) cells lose proper cell proportions and body axes.....	37
Figure 15	Cell shape analysis of control and Mob1(RNAi) cells shows a loss of normal proportions .....	39

Figure 16	The Mob1(RNAi) phenotypes are specific to the Mob1 sequence...	41
Figure 17	Mob1(RNAi) disrupts normal cell division .....	42
Figure 18	Progression of the Mob1(RNAi) phenotype .....	43
Figure 19	Presence of residual Mob1 protein in Mob1(RNAi) cells .....	45
Figure 20	Morgan revisited: regeneration of proportionate structures in <i>Stentor</i> requires Mob1 protein .....	48
Figure 21	Residual Mob1 in the anterior and posterior can be surgically removed.....	51
Figure 22	Reappearance of Mob1 in regenerating cells .....	52
Figure 23	Using ddPCR to determine copy number in <i>Stentor</i> .....	57
Figure 24	Gene copy number in <i>Stentor</i> .....	59
Figure 25	rDNA copy number scales with cell size .....	62
Figure 26	Wild isolates of <i>Stentor</i> .....	64
Figure 27	Features of <i>Stentor</i> during growth and division .....	67
Figure 28	Conjugation in wild <i>Stentor</i> .....	72

## Chapter 1: Introduction to *Stentor coeruleus*

Over the last few decades scientists have often turned to one of a handful of well-established model systems in order to ask any number of questions about how all of biology functions. This is absolutely useful and at the time that many of these systems were adopted the state of the art technologies were much more limited which made it much more efficient to focus on just a few organisms to set the scientific standards. However, recently there have been many advances in technology that have allowed for the relatively quick development of new and interesting model organisms. This should allow scientists to tailor what we are working on with the types of questions we want to address without being limited to the handful of established models. The questions I seek to address are those related to morphogenesis and pattern formation

*Stentor* was first described in 1744 by Abraham Trembley, although he did not coin the name *Stentor*, and it has a complex morphology, large cell size, and long history as a classical system for studying regeneration in single cells (Fig. 1A) [1]. *Stentor coeruleus*, like other ciliate organisms, is covered in cilia that are used for locomotion. These cilia are organized into rows along anterior/posterior axis of the cortex, and these rows are asymmetrically spaced along the circumference of the cell to define a dorsal/ventral axis. *Stentor* is a filter feeder, which uses its oral apparatus (OA), a dense band of cilia around the anterior of the cell, to sweep other living cells into its mouth. It is known to feed on bacteria, algae, and even other ciliates [2]. At the posterior, *Stentor* possesses an anchoring structure known as the holdfast, or foot, which is used to transiently attach to surfaces. Like other ciliates, *Stentor* is binucleate, and contains both a micronucleus as well as a macronucleus. While there is minimal

Figure 1: The anatomy of *Stentor coeruleus*.

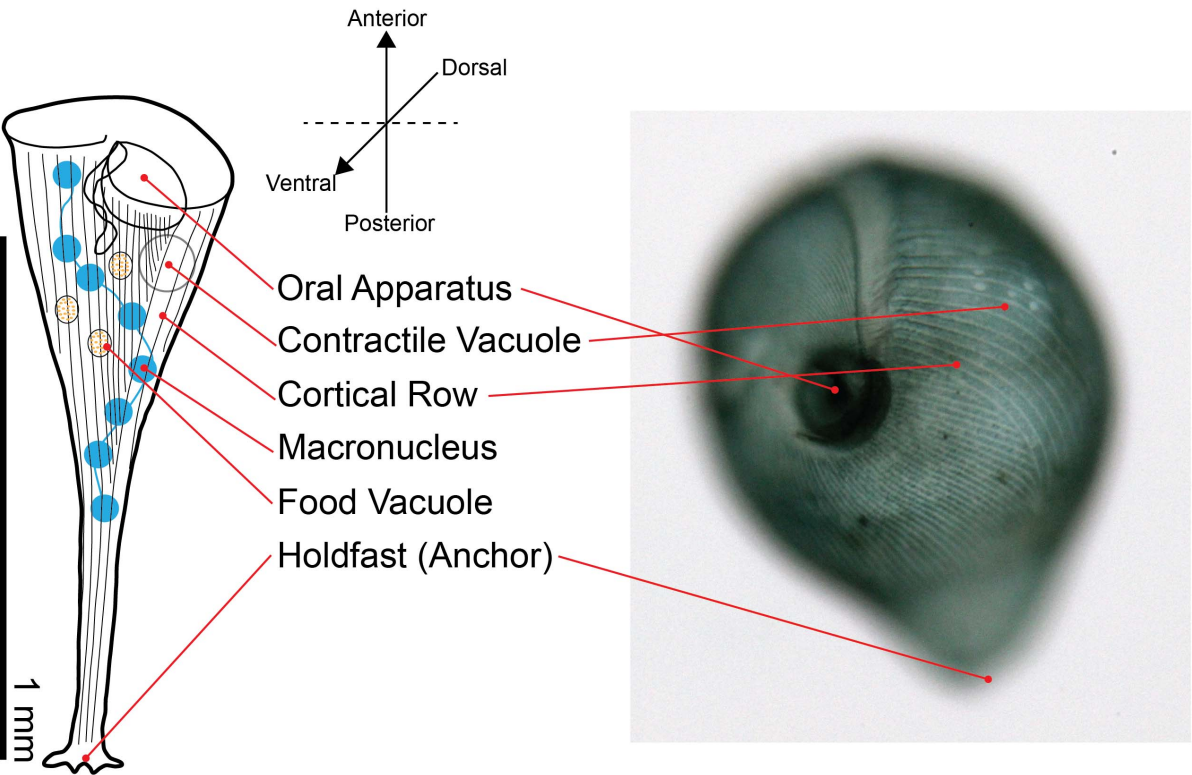


Figure 1. Cartoon of *Stentor coeruleus* highlighting key cellular structures, all of which have reproducible positions within the cell.

information about the micronucleus in *Stentor*, the macronucleus is moniliform, which means that it has the shape of beads on a string, and forms multiple nodes that are stretched across the length of the cell that are generally physically connected to one another. Given the complexity of *Stentor*'s anatomy along with the immense size of the organism it is often shocking to imagine how it can exist as only a single cell.

In addition to the physical complexity, *Stentor* also displays a number of complex behaviors, most of which are well detailed in Tartar's book but I will cover briefly here[2]. In their basal state the cells anchor to a substrate via their holdfast and extend their cell bodies out into the environment to feed, giving the cells their canonical trumpet shape. While they are extended the cells are able to bend and contort themselves in a well-controlled fashion. Additionally, *Stentor* is mechanosensitive and will contract its cell body down into a ball if stimulated by physical forces. If they are perturbed enough the cells will detach and swim around in a partially contracted shape and eventually find a new location to anchor. In addition to mechanosensitivity, the cells are also light sensitive and will generally settle in a location with relatively low light, although the specific mechanism for their light sensation is unknown[3].

Even *Stentor*'s capacity to consume food is interesting and could even be potentially useful as a vector for RNA interference (discussed later in Chapter 2) or other purposes. *Stentor* can consume enough food to fill vacuoles that are nearly the size of the entire cell body in a matter of minutes if the prey organism is concentrated enough (Figure 2A). In an attempt to develop an easy way to concentrate the cells and isolate them away from other contaminants I fed the cells magnetotactic bacteria,

Figure 2: *Stentor* is an efficient filter feeder and its prey may be used as a vector.

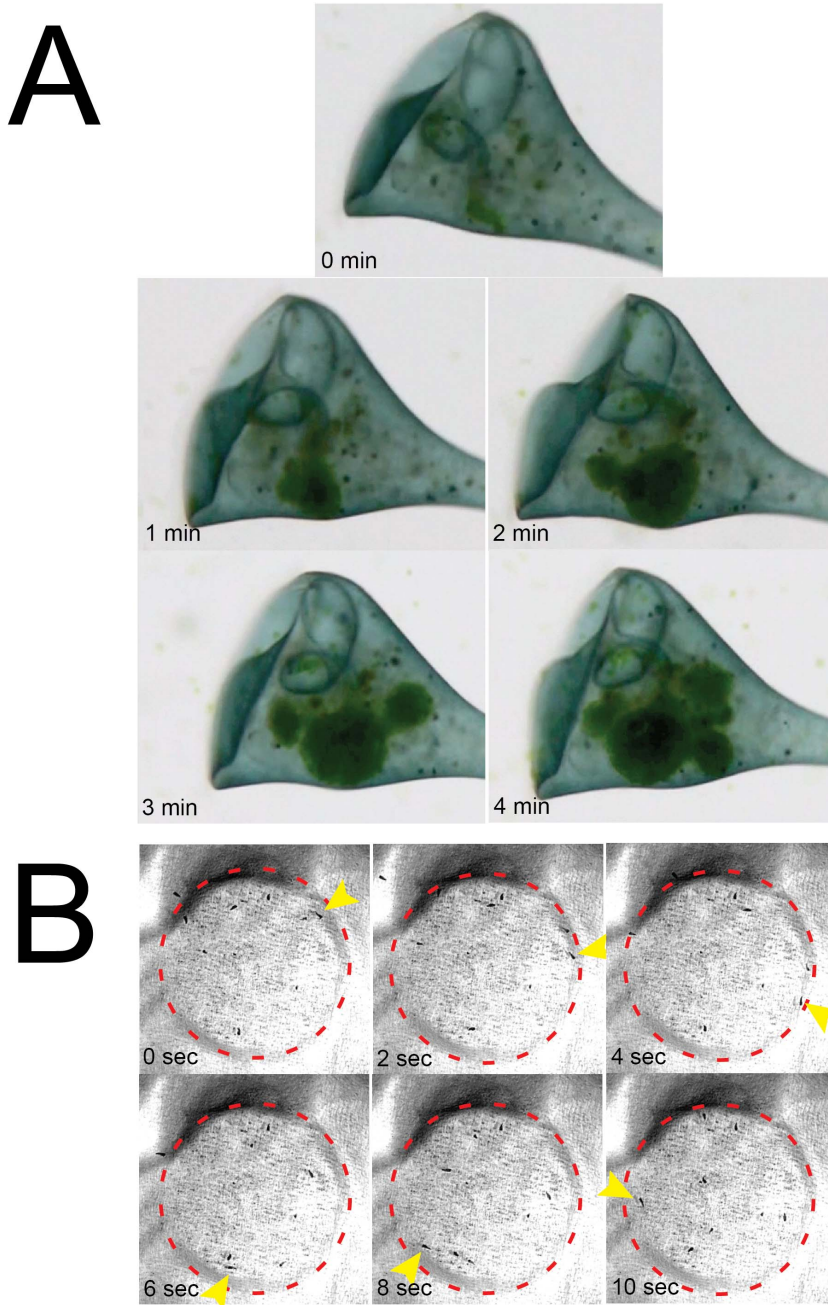


Figure 2. **(A)** Upon receiving a dose of *Chlamydomonas*, *S. coeruleus* is able to effectively and quickly capture large amounts of food to then digest. **(B)** If fed other organisms such as the magnetotactic bacteria, *Magnetospirillum*, within 30 minutes *Stentor* (yellow arrows) become magnetic and are able to be directed within magnetic



fields (edge of the magnet is indicated with a dashed red circle). However, after 2-4 hours the cells begin to digest and export the bacteria and are no longer magnetic.

although I assume magnetic beads would also work, and this caused the cells to become magnetic and I could bias their swimming by applying a magnetic field (Figure 2B). Although ultimately not useful for my purposes because the cells could not be held still and were actually able to escape the magnetic field, it serves as a good proof of principle that something along these lines could be used as assays for future experiments.

In addition to these simple behaviors, *Stentor coeruleus* also contains a blue/green pigment, called stentorin, that functions as a defense mechanism. These pigments are densely packed into granules and held near the cell surface that are easily seen in EM studies [4]. Under conditions of stress *Stentor coeruleus* rapidly secretes large amounts of this pigment into the environment, similar to a squid inking the water. Although the exact mechanism is unknown, stentorin is a toxin that either kills or deters predators that threaten *Stentor* [5]. Interestingly, stentorin is also fluorescent and can be visualized using a standard rhodamine filter (555nm Ex / 617nm Em) [6]. However, I found that the pigment appears to be in a quenched state when inside the pigment granules but it becomes highly fluorescent upon release into the extracellular environment, which allowed me to visualize what appear to be single vesicle fusion events in real time (Figure 3A). Unfortunately, the stentorin fluorescence is a problem when preparing *Stentor coeruleus* samples for immunofluorescence because the stentorin molecule seems to be released from the pigment granules and labels nearly the entire cell volume, causing it to become brightly fluorescent and renders any fluorescent secondary antibodies whose spectra overlap with stentorin useless (Figure 3B).

**Figure 3: Stentorin secretion and autofluorescence.**

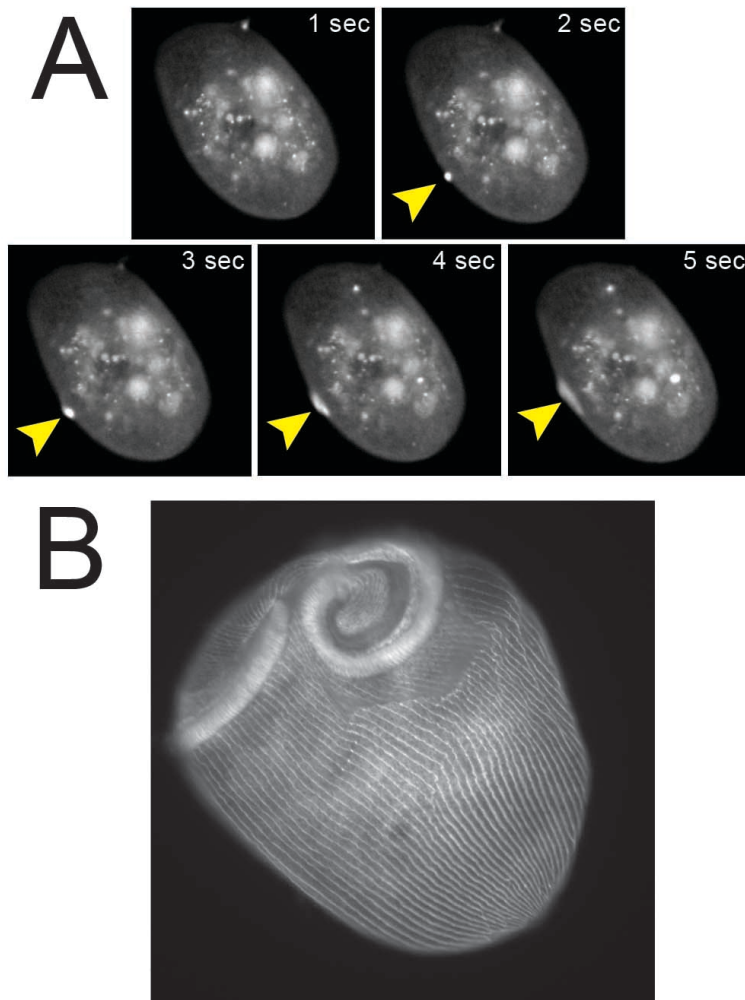


Figure 3. **(A)** Under stress conditions *Stentor coeruleus* secretes a toxic pigment called stentorin as a defense mechanism. Stentorin becomes highly fluorescent when it is released from the dense pigment granules where it is normally stored at the cell surface. Here you can see a single granule being secreted and then the pigment gets rapidly diffused by the action of the cilia (arrows). **(B)** After methanol fixation stentorin becomes extremely fluorescent and stains the entire cell volume as well as many of the structures of the cell.

But perhaps some of their most interesting behavioral capabilities are the ability to learn and the ability to regenerate. Using contraction due to mechanical stimulation as a readout, *Stentor* has been shown to habituate to frequently repeated stimuli within 20 or 30 minutes[7]. The mechanism that allows for this learning behavior has not yet been identified but the work of David C. Wood has gone a long way of describing this phenomenon[8]. *Stentor* could be a very powerful model for determining how single cells might have the ability to learn/habituate in ways that have previously only been considered in metazoans.

Finally, *Stentor* can regenerate from almost any injury and it is this process that fascinated scientists more than a century ago and what attracted me to the system [9]. Given the cell's immense size, *Stentor* is quite amenable to manual surgical manipulations which allowed Vance Tartar to perform a multitude of different styles of surgery as well as grafting in order to define many of the basic principles of morphogenesis [2]. Importantly, this is not simply a process of resealing the membrane and healing from a physical injury. These cells have some uncharacterized mechanism of sensing the specific parts of their anatomy and when any of these parts are absent the cell initiates a program of regenerating only those missing features and does so in a way that maintains proper cell proportions (Figure 4). This presents a number of interesting questions to attempt to answer: How does the cell maintain its integrity during and after injury? What mechanism is in place to identify that the cell is intact? How does a cell know specifically which portions are missing? How is the complex morphology regenerated in such a proportional and faithful manner? Are any of the morphological properties of *Stentor* applicable to other Eukaryotes?

Figure 4: Regeneration of proportionate structures in *S. coeruleus*.

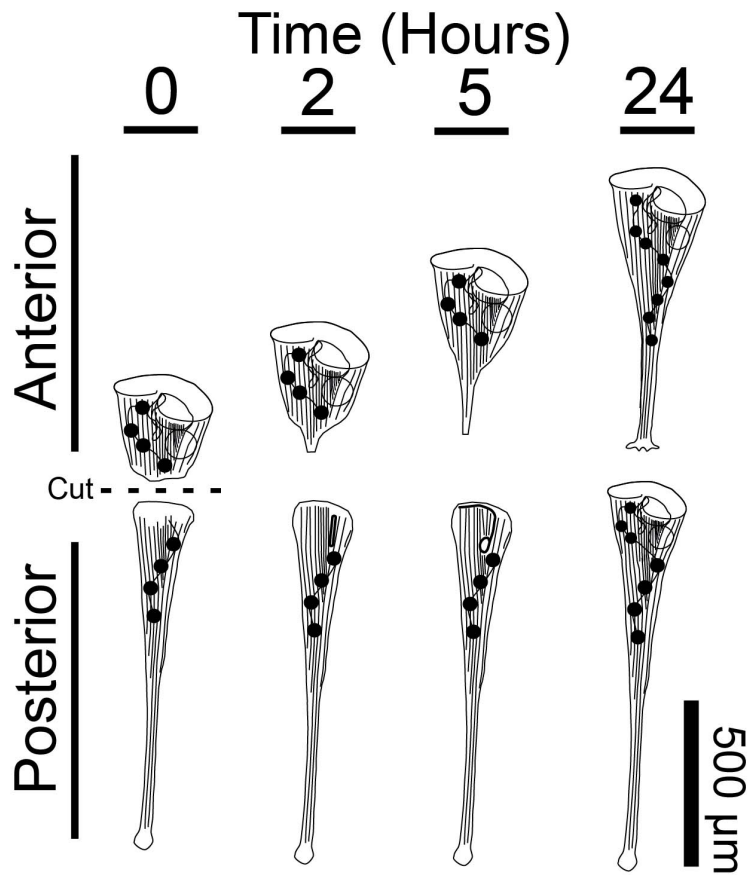


Figure 4. Cartoon representing *Stentor* regeneration after surgical bisection as initially reported by Thomas Hunt Morgan in 1901.

For all of these reasons I was drawn to working on *Stentor coeruleus* in order to learn more about its morphogenesis and ability to regenerate. However, when I began there were no cell or molecular biology labs working on morphogenesis in *Stentor*, and there had not been for decades. That majority of the microsurgical work was performed in the 1960s and 1970s by only two scientists, Vance Tartar and Noël de Terra; both of whom had unfortunately passed away. Thus, I was forced to relearn many of the classic methods from sometimes-vague descriptions in the literature and also develop many of the basic methods for working with *Stentor* myself. This certainly presented a unique challenge but I feel that given the current state of technology it is the perfect time to revisit *Stentor coeruleus* as a modern model organism for morphogenesis, regeneration, and even habituation!

The ability to develop and regenerate complex morphologies from a simpler starting point are among the properties that set living organisms apart from inanimate matter. Although these processes are most often considered in the context of embryos and multicellular organisms, even individual cells need to develop and regenerate after injury. Metazoan development is conceptually straightforward, in that organisms rely on the existence of numerous individual cells that differentiate into various cell types with specialized functions, thereby creating the complex architecture of the larger organism. However, it is less clear how similar levels of complexity can exist in an individual cell that cannot rely on the differentiation of its subunits. The morphogenesis of individual cells represents a key process in cell and developmental biology, but its mechanisms are almost completely unknown [10, 11].

To understand the fundamental features of complex morphogenesis we need a model where it can be induced in the context of a single cell. In some cases the process of regeneration mimics that of morphogenesis, so a single cell model for regeneration could be a very powerful tool. For this reason, we turned to the large ciliate *Stentor coeruleus* (~ 1mm long). The large size of *Stentor* cells made them amenable for surgical manipulations such as cutting and grafting, allowing experimental approaches comparable to those of experimental embryology to be applied to the study of single cells. The OA and holdfast, along with ciliated stripes that run the length of the organism, define the cell cortex and set up the anterior-posterior, dorsal-ventral, and left-right axes, that are maintained throughout division. *Stentor* thus displays complex patterning and axiation comparable to what is seen in embryos. Perhaps the most striking property of *Stentor* is that it has the ability to regenerate an entire normal organism from only a fraction of the original cell.

Its large size, complex architecture, ease of surgical manipulations, and ability to regenerate give *Stentor* significant advantages over other ciliate models and even made it the focus of some early embryologists. Thomas Hunt Morgan showed that surgically produced cell fragments could regenerate into properly proportioned cells (Figure 4), arguing that regeneration in *Stentor* was a strictly controlled morphological process [9]. The study of *Stentor* reached its apotheosis in the work of Vance Tartar, who made extensive use of microsurgery to understand the basic principles of morphogenesis in *Stentor* [2]. Tartar showcased the robust nature of *Stentor*'s regenerative ability in minceration experiments that disrupted the polarity of the cortex but did not prevent the cells from re-establishing normal polarity [12]. He also grafted parts of cells to one

another to show that a single region of the cell known as the locus of stripe contrast could control the formation of a new body axis [13]. The ability to induce the regeneration of specific cellular structures is a major advantage of *Stentor* as a model for morphogenesis [14-16]. But *Stentor* was never developed as a molecular model system and thus, despite ongoing fascination with the question of how a cell can develop such complexity, the molecular basis of pattern formation and regeneration in *Stentor* remains unknown.

Here we demonstrate that RNA interference (RNAi) technology is highly effective in *Stentor*, thus enabling us to study molecular mechanisms of *Stentor* development. For our initial attempt to use RNAi to identify a molecular determinant of morphogenesis in *Stentor*, we noted that the sequence of morphological events that take place when the cell regenerates a new oral apparatus is virtually identical to those observed when a cell forms a second oral apparatus during normal division [17]. We therefore used a candidate-based approach to delineate potential regulators of *Stentor* morphogenesis by focusing on conserved components of both cell division and polarization/morphogenesis. One potential candidate is the conserved eukaryotic kinase-regulator Mob1. Mob1p was first identified in budding yeast [18], and is part of a highly conserved family of which yeast has two members, Mob1p and Mob2p. Mob1p is involved in the mitotic exit network and is required for proper cytokinesis while Mob2p is involved in the regulation of Ace2p and polarized morphogenesis network and is required for proper cell morphology [19]. Mob1 is a highly conserved kinase co-activator that binds to NDR/LATS kinases and stimulates their activity. Mob1 has been implicated in the Hippo signaling pathway in *Drosophila* [20] and plays a role in a variety of processes including



apoptosis, mitosis, morphogenesis, and proliferation [21]. Recent work on the only member of the MOB family in *Tetrahymena thermophila* suggests that Mob1 function is conserved in ciliates and that Mob1 is required for proper cytokinesis, but it is unclear whether Mob1 functions in ciliate morphogenesis [22]. Here we show that Mob1 is conserved in *Stentor* and is asymmetrically localized in the cell. Using RNAi, we discovered that Mob1 is a global patterning protein that is required for proper development and regeneration.

## Chapter 2: RNA Interference in *Stentor coeruleus*

The *Stentor* genome is currently being assembled and annotated. In order to determine if the RNAi machinery is conserved in *Stentor coeruleus* prior to completion of the *Stentor* genome, we obtained genomic sequence using short Illumina reads that were assembled using the targeted assembly algorithm PRICE [23]. Using reads with homology to *Tetrahymena* proteins as seed sequences, we specifically assembled sequences with homology to known RNAi machinery such as Argonaute, Dicer, and RNA-dependent RNA polymerases (RdRP). We were able to assemble a number of homologs for each of the RNAi machinery components (Table 1). Using a recently reported functional analysis of the Argonaute homologs in *Paramecium* [24] as a reference point, we performed a neighbor-joining phylogenetic analysis of *Stentor* Argonaute homologs. Like those of *Paramecium* and other ciliates, all *Stentor* Argonaute proteins cluster in the PIWI subfamily (Figure 5); hence we use the term Sciwi for *Stentor coeruleus* PIWI. All of the Sciwi proteins contain the conserved “DDH” motif (Figure 6), which has been shown to be necessary for the slicer activity of PIWI proteins [25].

Based on the high sequence conservation of the RNAi machinery, we asked whether gene expression could be perturbed by RNAi in *Stentor*. RNAi has been performed in two other ciliates, *Paramecium tetraurelia* and *Blepharisma japonicum*, using the method of feeding with bacteria expressing double stranded RNA [26, 27]. However in other ciliates, such as *Tetrahymena thermophila*, RNAi by feeding does not work. To test whether RNAi by feeding is effective in *Stentor*, we performed a knockdown of  $\alpha$ - and  $\beta$ -tubulin – key components of the cortical structures in *Stentor* –

**Figure 5: Phylogenetic tree of *S. coeruleus* Sciwi proteins.**

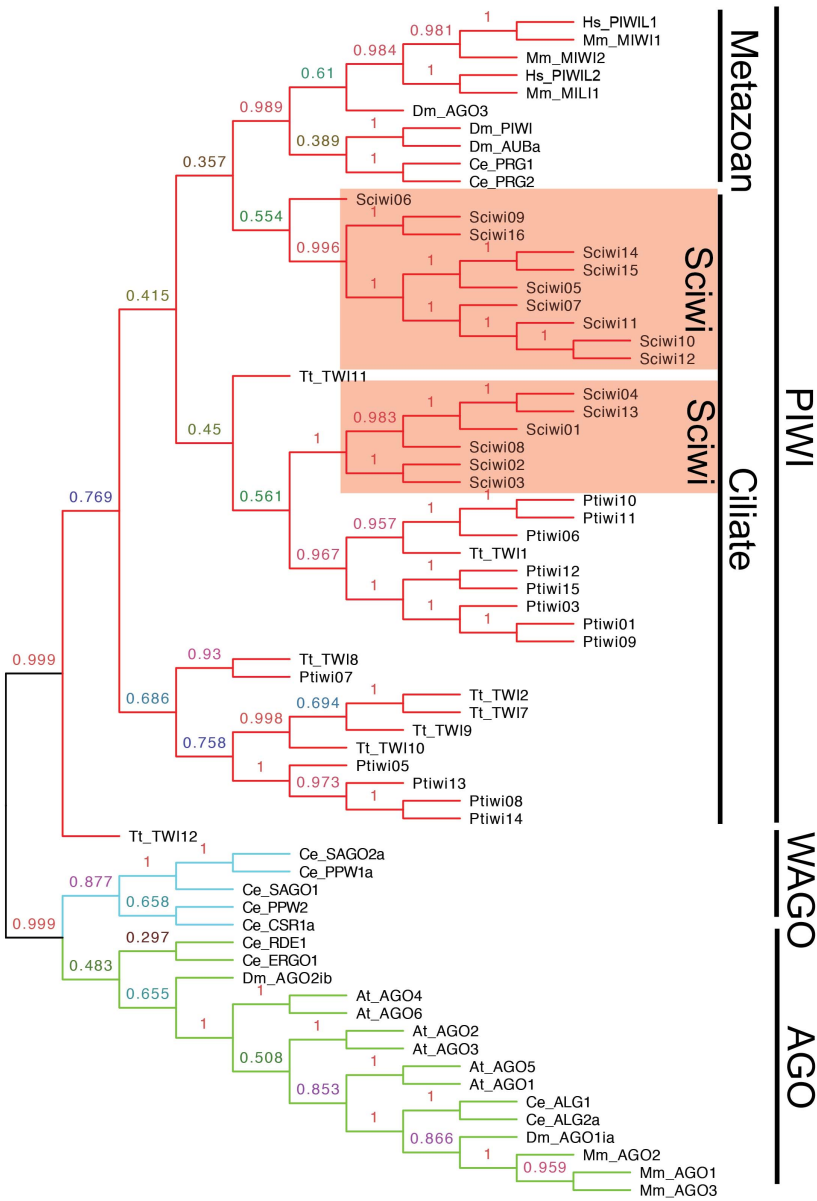


Figure 5. A neighbor-joining phylogenetic analysis of protein sequences of *Stentor argonaute* homologs along with sequences from *Paramecium* (*Pt*), *Tetrahymena* (*Tt*), human (*Hs*), mouse (*Mm*), *C. elegans* (*Ce*), *Drosophila* (*Dm*) and *Arabidopsis* (*At*). The three major classes of Argonaute proteins, PIWI, WAGO, and AGO are indicated (Sciwi proteins listed in Table 1, gene IDs in Table 2).

**Table 1: List of homologs of RNAi machinery found in the *S. coeruleus* genome.**

Gene Name	GenBank Accession #	Top Hit [Paramecium]	E-Value
Sciwi01	KJ649660	<a href="#">GSPATG00002500001</a>	4.00E-114
Sciwi02	KJ649661	<a href="#">GSPATG00019939001</a>	4.00E-133
Sciwi03	KJ649662	<a href="#">GSPATG00009468001</a>	4.00E-134
Sciwi04	KJ649663	<a href="#">GSPATG00009468001</a>	8.00E-121
Sciwi05	KJ649664	<a href="#">GSPATG00036761001</a>	7.00E-99
Sciwi06	KJ649665	<a href="#">GSPATG00036761001</a>	7.00E-91
Sciwi07	KJ649666	<a href="#">GSPATG00036761001</a>	2.00E-115
Sciwi08	KJ649667	<a href="#">GSPATG00009468001</a>	3.00E-119
Sciwi09	KJ649668	<a href="#">GSPATG00016237001</a>	7.00E-84
Sciwi10	KJ649669	<a href="#">GSPATG00036761001</a>	4.00E-117
Sciwi11	KJ649670	<a href="#">GSPATG00036761001</a>	3.00E-114
Sciwi12	KJ649671	<a href="#">GSPATG00036761001</a>	6.00E-109
Sciwi13	KJ649672	<a href="#">GSPATG00009468001</a>	4.00E-123
Sciwi14	KJ649673	<a href="#">GSPATG00036761001</a>	4.00E-109
Sciwi15	KJ649674	<a href="#">GSPATG00036761001</a>	4.00E-109
Sciwi16	KJ649675	<a href="#">GSPATG00016237001</a>	9.00E-84
DCR01	KJ649676	<a href="#">GSPATG00033115001</a>	2.00E-43
DCR02	KJ649677	<a href="#">GSPATG00003051001</a>	2.00E-18
DCR03	KJ649678	<a href="#">GSPATG00003051001</a>	4.00E-17
DCR04	KJ649679	<a href="#">GSPATG00003051001</a>	6.00E-17
DCR05	KJ649680	<a href="#">GSPATG00003051001</a>	3.00E-20
DCR06	KJ649681	<a href="#">GSPATG00003051001</a>	5.00E-23
RdRP01	KJ649682	<a href="#">GSPATG00024768001</a>	9.00E-89
RdRP02	KJ649683	<a href="#">GSPATG00024768001</a>	7.00E-80
RdRP03	KJ649684	<a href="#">GSPATG00024768001</a>	5.00E-72
RdRP04	KJ649685	<a href="#">GSPATG00036857001</a>	1.00E-72
RdRP05	KJ649686	<a href="#">GSPATG00036857001</a>	6.00E-72
BTU01	KJ649687	<a href="#">GSPATG00036831001</a>	0.00E+00
BTU02	KJ649688	<a href="#">GSPATG00036831001</a>	0.00E+00
BTU03	KJ649689	<a href="#">GSPATG00036831001</a>	0.00E+00
BTU04	KJ649690	<a href="#">GSPATG00036831001</a>	0.00E+00
BTU05	KJ649691	<a href="#">GSPATG00036831001</a>	0.00E+00
BTU06	KJ649692	<a href="#">GSPATG00036831001</a>	0.00E+00
ATU01	KJ649693	<a href="#">GSPATG00020765001</a>	0.00E+00
ATU02	KJ649694	<a href="#">GSPATG00020765001</a>	0.00E+00
ATU03	KJ649695	<a href="#">GSPATG00002927001</a>	0.00E+00
ATU04	KJ649696	<a href="#">GSPATG00002927001</a>	0.00E+00
ATU05	KJ649697	<a href="#">GSPATG00020765001</a>	0.00E+00
ATU06	KJ649698	<a href="#">GSPATG00002927001</a>	0.00E+00
ATU07	KJ649699	<a href="#">GSPATG00020765001</a>	0.00E+00
ATU08	KJ649700	<a href="#">GSPATG00002927001</a>	0.00E+00
Mob1a	KJ649653	<a href="#">GSPATG00019838001</a>	6.00E-125
Mob1b	KJ649654	<a href="#">GSPATG00019838001</a>	4.00E-126
Mob1c	KJ649655	<a href="#">GSPATG00019838001</a>	6.00E-125
Mob1d	KJ649656	<a href="#">GSPATG00019838001</a>	7.00E-125
Mob1e	KJ649657	<a href="#">GSPATG00019838001</a>	6.00E-125
Mob1f	KJ649658	<a href="#">GSPATG00019838001</a>	6.00E-125
Phocein	KJ649659	<a href="#">GSPATG00005136001</a>	2.00E-85

Table 1. List of identified RNAi machinery homologs in *Stentor*. Argonaute (Sciwi), Dicer, and RNA-dependant RNA polymerases were identified from genomic sequence using a best-reciprocal BLAST approach starting with annotated *Paramecium tetraurelia* proteins. For each gene the Genbank accession number and the top hit in *Paramecium* is also shown with its corresponding E-value.

**Table 2: Gene IDs for RNAi machinery used in phylogenetic analysis of Sciwi proteins.**

Branch name	Gene ID	Gene/Species
>Ptiwi13	GSPATP00016237001	Ptiwi13 [Paramecium tetraurelia]
>Ptiwi12	GSPATP00001709001	Ptiwi12 [Paramecium tetraurelia]
>Ptiwi10	GSPATP00009468001	Ptiwi10 [Paramecium tetraurelia]
>Ptiwi07	GSPATP00009544001	Ptiwi07 [Paramecium tetraurelia]
>Ptiwi06	GSPATP00002500001	Ptiwi06 [Paramecium tetraurelia]
>Ptiwi05	GSPATP00038263001	Ptiwi05 [Paramecium tetraurelia]
>Ptiwi03	GSPATP00001395001	Ptiwi03 [Paramecium tetraurelia]
>Ptiwi01	GSPATP00021895001	Ptiwi01 [Paramecium tetraurelia]
>Ptiwi08	GSPATP00021288001	Ptiwi08 [Paramecium tetraurelia]
>Ptiwi09	GSPATP00020796001	Ptiwi09 [Paramecium tetraurelia]
>Ptiwi11	GSPATP00019939001	Ptiwi11 [Paramecium tetraurelia]
>Ptiwi14	GSPATP00036761001	Ptiwi14 [Paramecium tetraurelia]
>Ptiwi15	GSPATP00005370001	Ptiwi15 [Paramecium tetraurelia]
>PIWIL1	gi 66346725 ref NP_004755.2	piwi-like protein 1 isoform 1 [Homo sapiens]
>PIWIL2	gi 33411132 dbj BAC81342.1	PIWIL2 [Homo sapiens]
>At_AGO4	gi 18401305 ref NP_565633.1	argonaute 4 [Arabidopsis thaliana]
>At_AGO2	gi 145336300 ref NP_174413.2	Argonaute family protein [Arabidopsis thaliana]
>At_AGO3	gi 15221662 ref NP_174414.1	protein ARGONAUTE 3 [Arabidopsis thaliana]
>At_AGO5	gi 30683679 ref NP_850110.1	Argonaute family protein [Arabidopsis thaliana]
>At_AGO6	gi 42569579 ref NP_180853.2	argonaute 6 [Arabidopsis thaliana]
>Mm_AGO1	gi 251823852 ref NP_700452.2	protein argonaute-1 [Mus musculus]
>Mm_AGO2	gi 219842353 ref NP_694818.3	protein argonaute-2 [Mus musculus]
>Mm_AGO3	gi 240120065 ref NP_700451.2	protein argonaute-3 [Mus musculus]
>Mm_MIWI1	gi 16905061 gb AAL31014.1	AF438405_1 MIWI [Mus musculus]
>Mm_MIWI2	gi 26449041 gb AAN75583.1	Miwi 2 protein [Mus musculus]
>Mm_MILI1	gi 7416113 dbj BAA93706.1	MILI [Mus musculus]
>Dm_AGO1a	gi 24653501 ref NP_725341.1	Argonaute-1, isoform A [Drosophila melanogaster]
>Dm_AGO2ib	gi 24664664 ref NP_648775.1	argonaute 2, isoform B [Drosophila melanogaster]
>Dm_PIWI	gi 17136736 ref NP_476875.1	piwi [Drosophila melanogaster]
>Dm_AUBa	gi 17136494 ref NP_476734.1	aubergine, isoform A [Drosophila melanogaster]
>Dm_AGO3	gi 126842396 gb ABO27430.1	Argonaute3 [Drosophila melanogaster]
>Tt_TWI1	gi 118370188 ref XP_001018296.1	Piwi domain containing protein [Tetrahymena thermophila]
>Tt_TWI2	gi 112386010 gb ABI17944.1	Twi2p [Tetrahymena thermophila]
>At_AGO1	gi 30694320 ref NP_849784.1	protein argonaute [Arabidopsis thaliana]
>Tt_TWI7	gi 145411516 gb ABP68416.1	Twi7p [Tetrahymena thermophila]
>Tt_TWI8	gi 112361408 gb ABI15747.1	Twi8p [Tetrahymena thermophila]
>Tt_TWI9	gi 158344559 gb ABW36050.1	PIWI-like Twi9p [Tetrahymena thermophila]
>Tt_TWI10	gi 145411514 gb ABP68415.1	Twi10p [Tetrahymena thermophila]
>Tt_TWI11	gi 158344561 gb ABW36051.1	PIWI-like Twi11p [Tetrahymena thermophila]
>Tt_TWI12	gi 389139313 gb ABP68417.2	Twi12p [Tetrahymena thermophila]
>Ce_ALG1	gi 25148113 ref NP_510322.2	Argonaute (plant)-Like Gene family member (alg-1) [Caenorhabditis elegans]
>Ce_ALG2a	gi 24418217 gb AAB66187.2	Argonaute (plant)-like gene protein 2, isoform a, partially confirmed by transcript evidence [Caenorhabditis elegans]
>Ce_ERGO1	gi 25148583 ref NP_503362.2	Protein ERGO-1 [Caenorhabditis elegans]
>Ce_RDE1	gi 25155102 ref NP_741611.1	Protein RDE-1 [Caenorhabditis elegans]
>Ce_PRG1	gi 17506389 ref NP_492121.1	Protein PRG-1 [Caenorhabditis elegans]
>Ce_PRG2	gi 17538380 ref NP_500994.1	Protein PRG-2 [Caenorhabditis elegans]
>Ce_CSR1a	gi 115532836 ref NP_001040938.1	Protein CSR-1, isoform a [Caenorhabditis elegans]
>Ce_SAGO1	gi 17562538 ref NP_504610.1	Protein SAGO-1 [Caenorhabditis elegans]
>Ce_SAGO2a	gi 17507671 ref NP_490758.1	Protein SAGO-2, isoform a [Caenorhabditis elegans]
>Ce_PPW1a	gi 25143854 ref NP_740835.1	Protein PPW-1, isoform a [Caenorhabditis elegans]
>Ce_PPW2	gi 7331726 gb IAAF60414.1	Paz/piwi domain-containing protein 2 [Caenorhabditis elegans]

Figure 6: Cartoon alignment of “DDH” motif in *S. coeruleus* PIWI-like proteins.

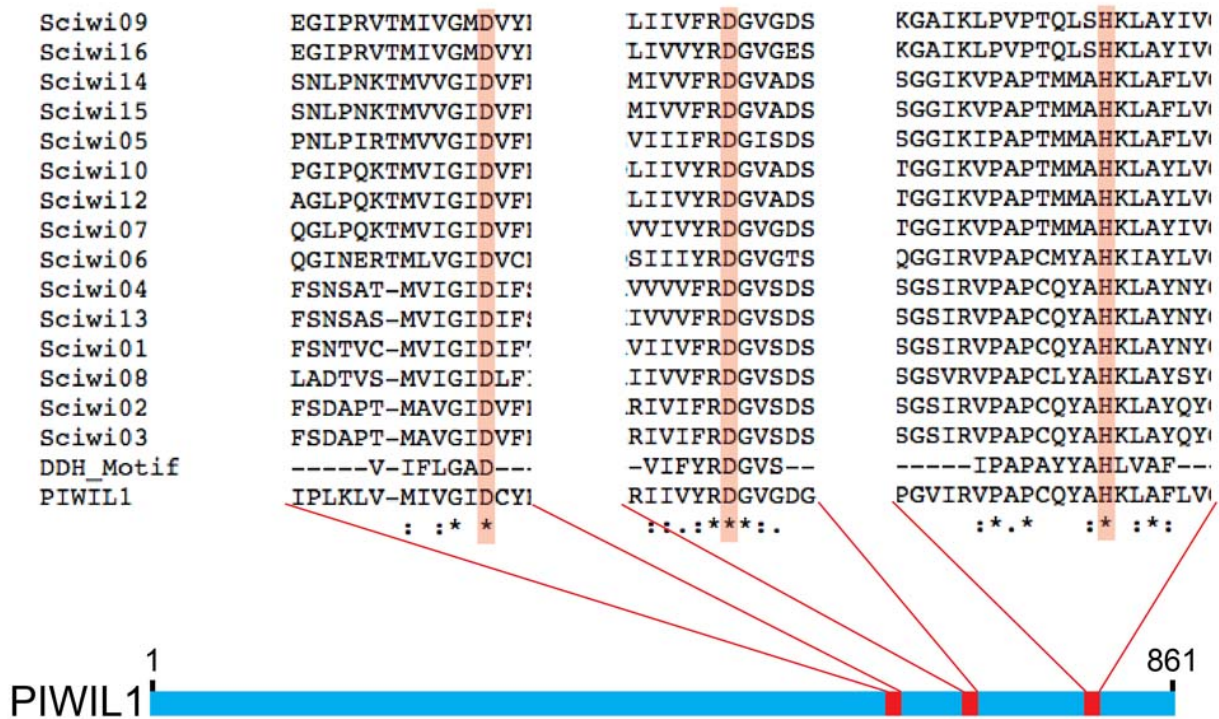


Figure 6. Multiple sequence alignment of the *Stentor* argonaute homologs with the canonical “DDH” motif and human PIWIL1, important residues are highlighted in red.

The alignment was performed using ClustalW2.

by feeding bacteria containing an expression plasmid encoding dsRNA directed against  $\alpha$ - or  $\beta$ -tubulin. There were eight  $\alpha$ -tubulin and six  $\beta$ -tubulin homologs identified from the PRICE assembly and at least one shared  $\geq 20$ mer among all of the sequences. We hypothesized that since tubulin is a key component of the cell structure its knockdown would display a clear phenotype as a proof of principle for RNAi. We found that RNAi resulted in a significant knockdown at the level of the transcript (Figure 7A). Targeting either  $\alpha$ - or  $\beta$ -tubulin with RNAi vectors caused cells to take on a rounded shape not seen in untreated cells after 5 days of feeding (Figure 7B, 7C, 8). Identical results were obtained targeting either tubulin gene or either half of the tubulin genes individually, arguing the result was not an off-target effect (Figure 8C). Using antibodies against  $\alpha$ -tubulin to highlight the cortical rows, we observed that tubulin knockdown resulted in the disorganization of cortical rows (Figure 7D, 7E). We also noted that the macronucleus in tubulin knockdown cells often collapsed into two large nodes, one located near the anterior and one at the posterior pole of the cell (Figure 8B). This failure to maintain an elongated macronucleus is consistent with a previous observation that microtubules are involved with elongation [28]. Cells depleted of tubulin appear to sustain cortical damage such as breaks and discontinuities of the cortical rows, which they are unable to repair properly (Figure 7E, arrows). Tartar found that cortical discontinuities induced by surgery often resulted in transient protrusions, resembling posterior poles, extending from the cell [12]. Consistent with that observation, we found that some tubulin knockdown cells formed ectopic posterior poles, suggesting a role for an organized cortex in the maintenance of cell polarity (Figure 8D).



Figure 7: *β-tubulin(RNAi)* results in aberrant cell morphologies.

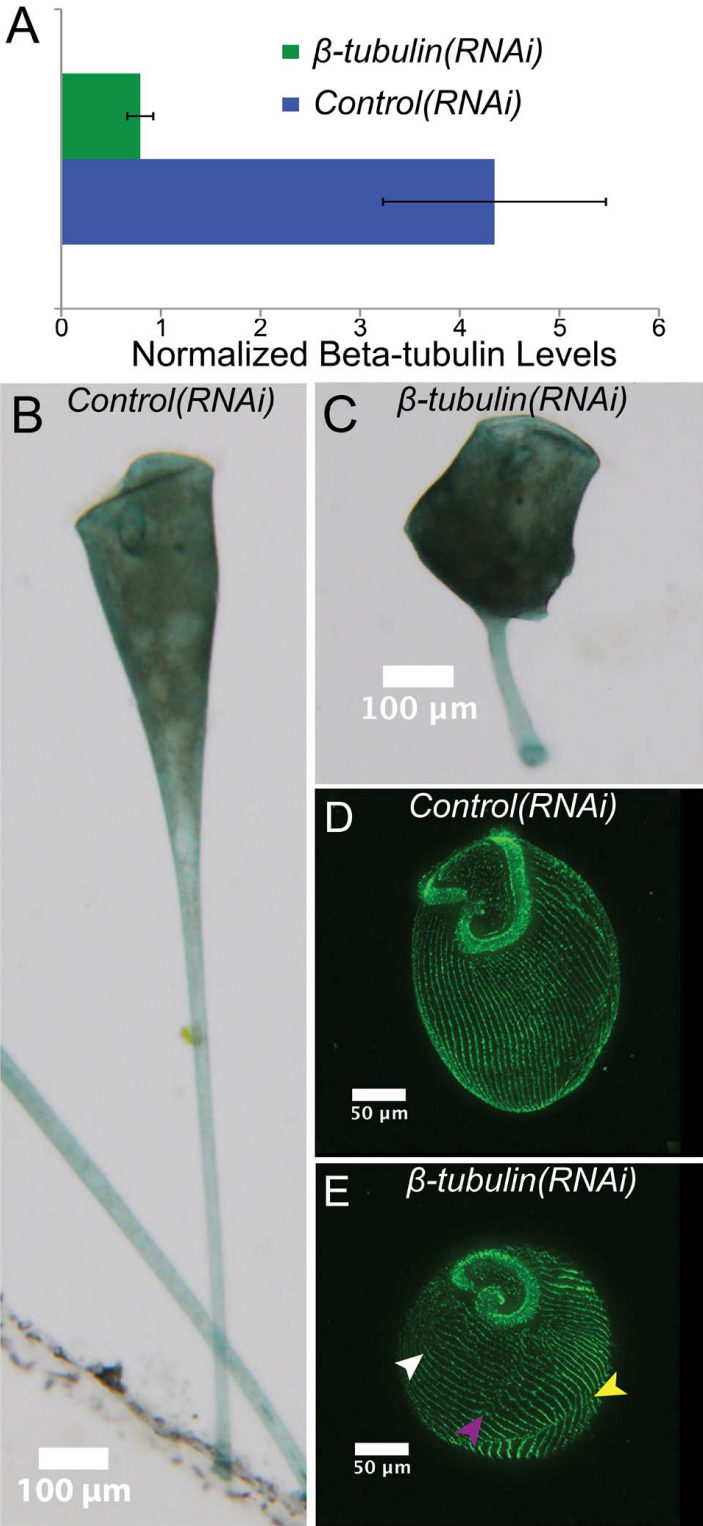


Figure 7. **(A)** qRT-PCR results showing relative expression of  $\beta$ -tubulin normalized to GAPDH expression in both *control(RNAi)* and  *$\beta$ -tubulin(RNAi)* cells. **(B, C)** Brightfield images of control and  *$\beta$ -tubulin(RNAi)* cells showing dramatic alteration in cell shape. **(D, E)** Immunofluorescence images of stained control and  *$\beta$ -tubulin(RNAi)* cells highlighting cortical microtubule bundles (green, anti- $\alpha$ -tubulin). In contrast to the highly organized parallel microtubule rows seen in control cells,  *$\beta$ -tubulin(RNAi)* cells have improperly oriented (white arrow), broken (purple arrow) and discontinuous (yellow arrow) rows, indicating a disruption of normal cellular patterning.

Figure 8: RNAi knockdown of  $\alpha$ - or  $\beta$ -tubulin yields similar morphological defects.

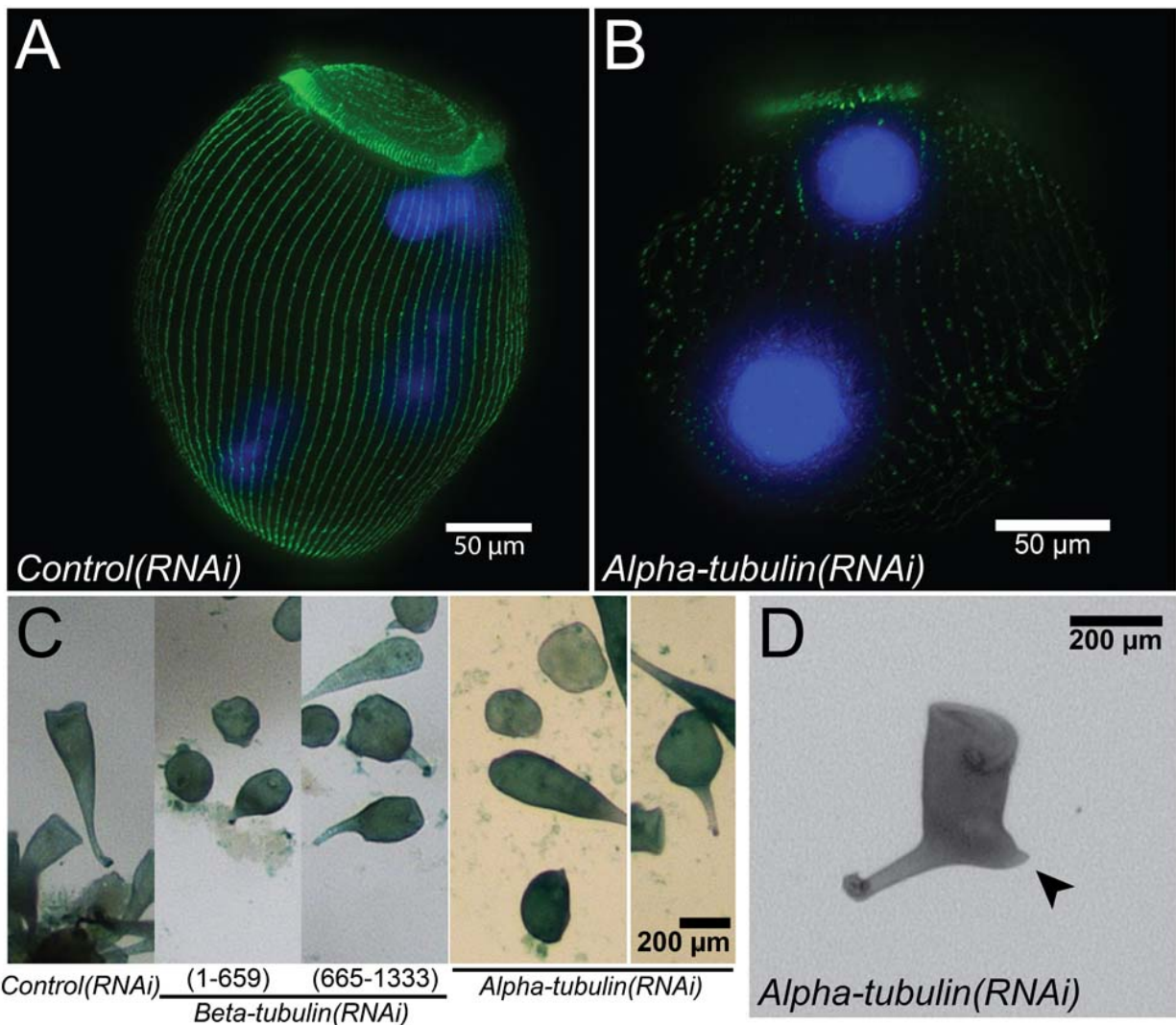


Figure 8. **(A)** Immunofluorescence image of a stained control cell; cortical rows (green, anti-acetylated-tubulin), macronucleus (blue, DAPI). **(B)** Immunofluorescence image of a stained  $\alpha$ -tubulin RNAi cell; cortical rows (green, anti-acetylated-tubulin), macronucleus (blue, DAPI). **(C)** Brightfield images of cells fed either control, split  $\beta$ -tubulin, or  $\alpha$ -tubulin vectors. **(D)** Brightfield image of an  $\alpha$ -tubulin RNAi cell that developed an ectopic posterior pole (arrow).

To demonstrate that the morphological defects seen in Figure 7 are specific for tubulin RNAi we performed RNAi using a gene whose function is predicted to be unrelated to cortical row organization, namely the ciliary length regulating kinase LF4 [29, 30]. When LF4 was knocked down via RNAi in *Stentor*, the cilia increased in length but tubulin staining of cortical rows, as well as cell shape and patterning were unaffected (Figure 7D, 9A-D). This result rules out the possibility that activation of the RNAi machinery causes nonspecific changes in cell morphology. Additionally, RNAi using sequences targeted to planarian ODF2 and unc22, genes not present in ciliates, resulted in normally shaped cells (Figure 9E, 9F). These data show that RNAi constitutes a powerful tool for studying the molecular mechanisms of regeneration and morphogenesis in *Stentor*.

**Figure 9: Control RNAi cells have normal morphologies.**

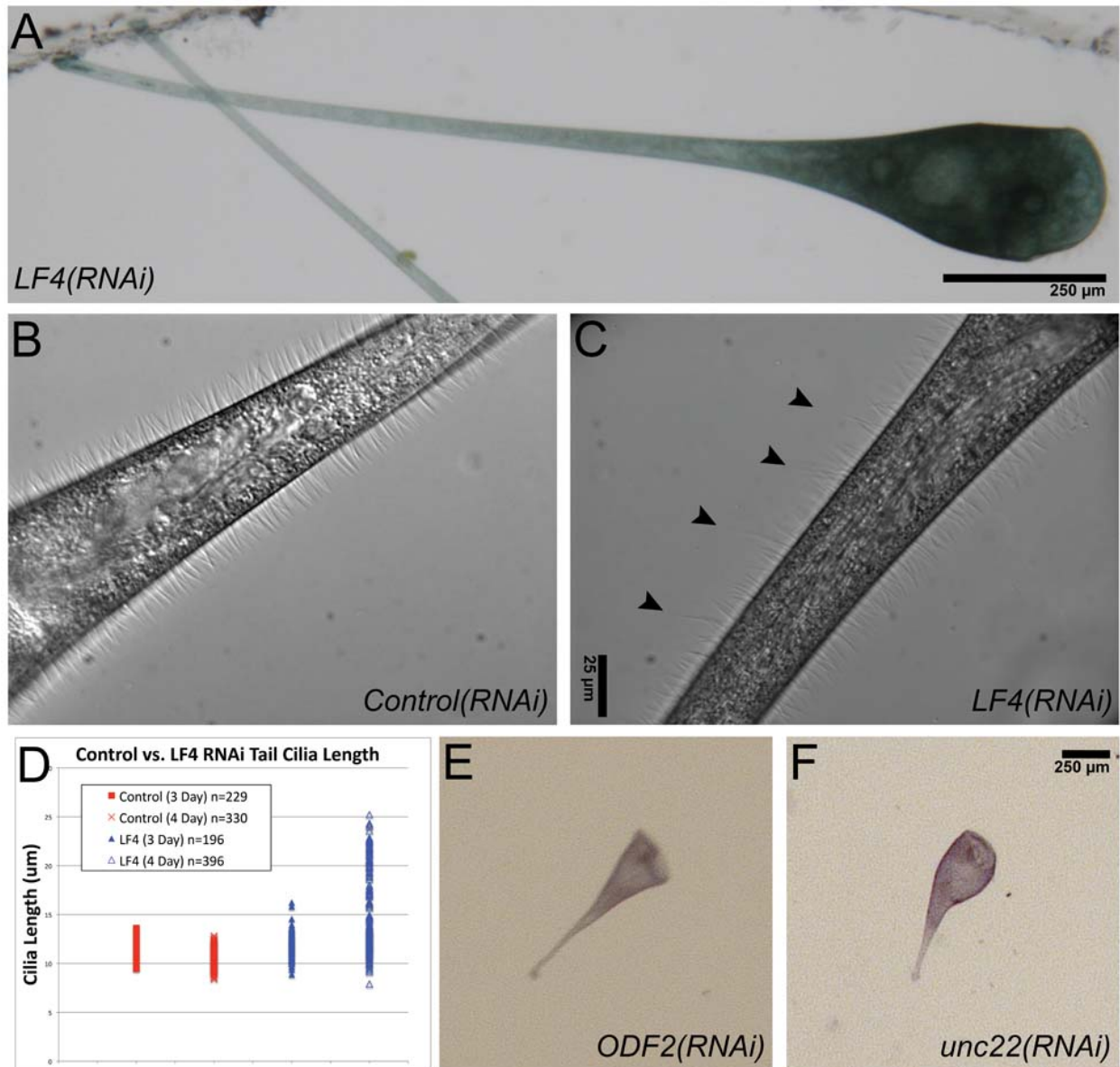


Figure 9. **(A)** Brightfield image of an *LF4(RNAi)* cell. *LF4* is a kinase involved in ciliary length control but not expected to play any role in cortical patterning. We identified 24 potential *LF4* homologs from the PRICE assembly using reciprocal-best-BLAST hits and cloned the top hit. As expected, cell shape was completely normal in the *LF4(RNAi)* cells. **(B, C)** DIC images of control and *LF4(RNAi)* cell's posterior region showing their

cilia, image taken at 40x. *LF4(RNAi)* cells have significantly longer cilia (arrows), confirming that RNAi of LF4 was effective. **(D)** Graph of cilia lengths for control and *LF4(RNAi)* cells after 3 and 4 days of feeding the RNAi vectors. **(E, F)** Brightfield images of both planarian *ODF2(RNAi)* and *C. elegans unc22(RNAi)*, genes not present in *Stentor*, which have no obvious phenotype.

### Chapter 3: Mob1 acts as a global patterning protein in *Stentor coeruleus*

Having established the efficacy of RNAi, we set out to use this method to test the function of a candidate morphological determinant, Mob1, based on the reasoning outlined in the introduction. From the targeted PRICE assembly we discovered a total of six genes with high homology to Mob1 (Figure 10A). A seventh sequence was identified with homology to Phoecin, a protein that shares the MOB/Phoecin domain that defines the family (Figure 10A). All six putative Mob1 homologs were 99% identical to each other at the protein level (Figure 10B) and shared 52% identity with Mob1 versus only 38% identity with Mob2 protein sequences from *S. pombe* and we refer to them as Mob1. To determine the localization of Mob1 in *Stentor*, we generated a polyclonal antibody against a *Stentor* Mob1 peptide sequence shared between all six identified proteins. On western blots of Mob1 immunoprecipitated from *Stentor* lysates, the affinity-purified *Stentor* Mob1 antibody recognized a single band of the appropriate size at 26 kDa (Figure 10C). When used for immunofluorescence, the antibody clearly labeled the posterior and appeared to label the region around the OA, although this staining was less clear (Figure 10D). This localization pattern was blocked by pre-incubating the primary antibody with the immunizing peptide, which suggested that it is specific to the Mob1 family and not the result of a non-specific antibody binding (Figure 11). This dual localization pattern was similar to the pattern seen in *Tetrahymena* [22]. Interestingly, unlike in *Tetrahymena*, the antibody did not appear to exclusively label basal bodies in *Stentor*, but rather diffusely labeled the cortical rows (Figure 10E).

**Figure 10: Conservation of Mob1 and its localization in *Stentor*.**

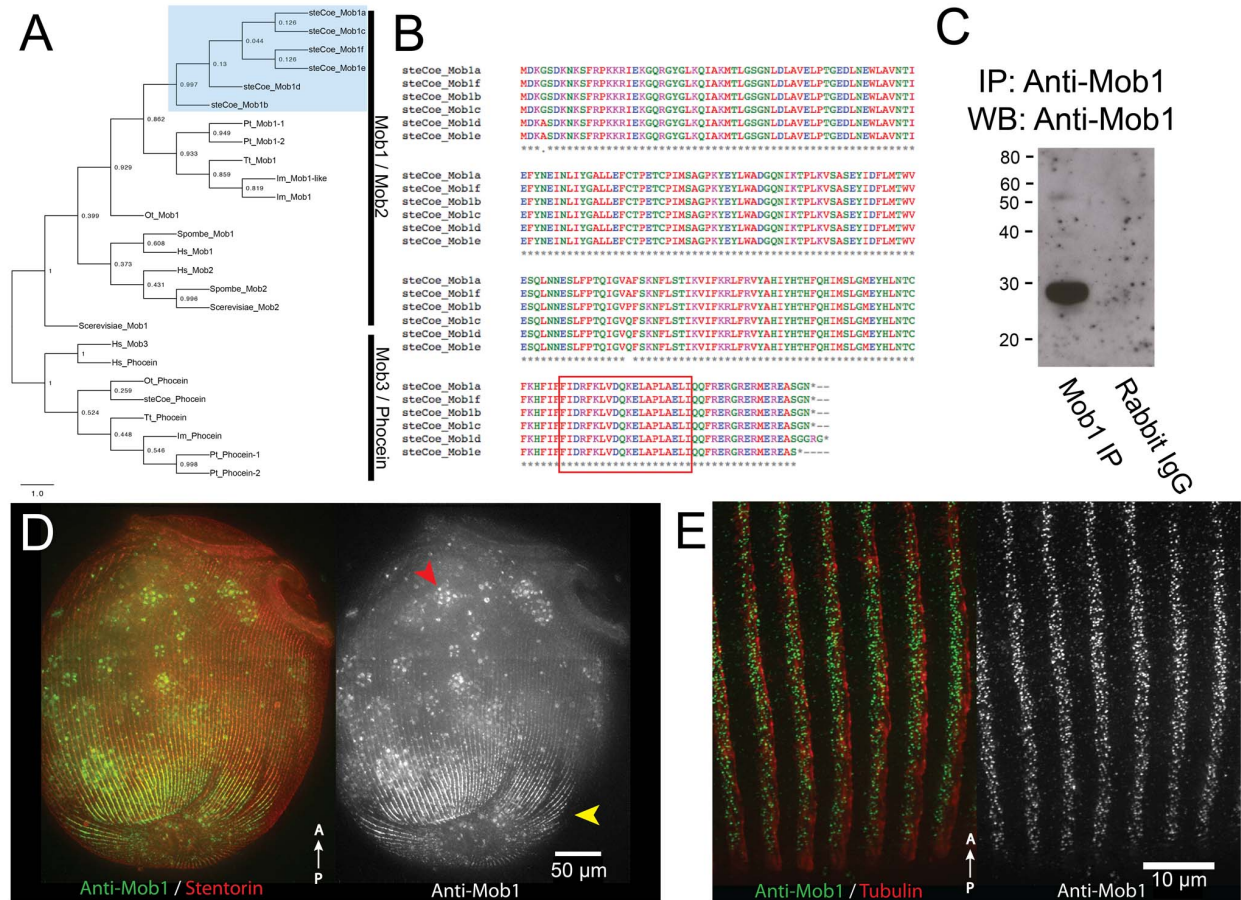


Figure 10. **(A)** Maximum-likelihood phylogenetic tree showing *Stentor* Mob1's position relative to other MOB family sequences from Human (Hs), *S. cerevisiae*, *S. pombe* (Sp), Tetrahymena (Tt), Paramecium (Pt), Ichthyophthirius (Im) and Oxytricha (Ot). Cluster of *Stentor* sequences is indicated with a blue box. **(B)** Alignment of *Stentor coeruleus* Mob1 protein sequences. The peptide sequence used to generate the Mob1 antibody is indicated by the boxed region near the C-terminus. **(C)** IP:Western blot showing the Mob1 band present at 26 kD. Rabbit IgG alone was run to gauge the level of background signal generated by the secondary antibody to rule out contaminating signal from IgG light-chain, which is around the same size as Mob1. **(D)** Immunofluorescence



image of cells showing Mob1 localization (green, anti-Mob1) and cortical rows (red, stentorin-autofluorescence). Mob1 localizes to the OA in the anterior, and cortical rows of the posterior (yellow arrow). There is background signal from autofluorescent food vacuoles containing *Chlamydomonas* (red arrow). **(E)** Immunofluorescence image showing a high magnification view of Mob1 localization (green, anti-Mob1) at the posterior, which is punctate and diffusely labels the cortical rows marked by the tubulin staining (red, anti-acetylated-tubulin).

Figure 11: Antibody against *S. coeruleus* Mob1 specifically recognizes its target.

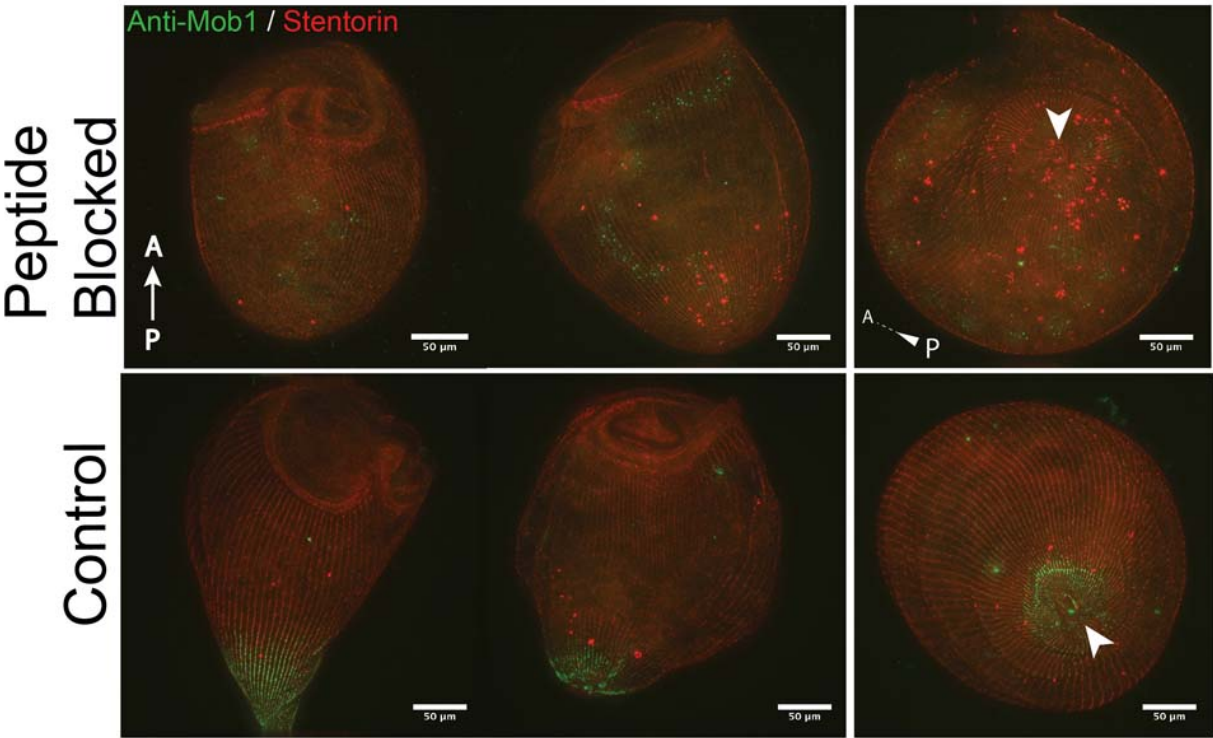


Figure 11. Immunofluorescence images showing that the signal in the posterior disappears when the anti-Mob1 antibody is pre-incubated with the immunizing peptide before staining. Under these conditions, punctate staining in the nucleus that dominates, suggesting that it is off-target or non-specific staining.

To get a better idea of Mob1 localization throughout the cell cycle we followed dividing cells and fixed them at different stages of division. Division proceeds through a series of 8 morphologically defined stages [2]. During stage 1 the oral primordium begins to form as a clearing of rows along the locus of stripe contrast at the midline of the cell, which expands during stage 2. In stages 3 and 4 this clearing is filled by the synthesis of new basal bodies, which are then ciliated as the oral primordium increases in length. In stage 5 the cell elongates as the oral primordium further develops and the macronucleus begins to condense. By stage 6 the macronucleus collapses into a single large node and cortical partitions between the anterior and posterior daughter cells become visible. Finally, during stages 7 and 8 the macronucleus extends back to its normal shape and is divided between the two daughters as the oral primordium is positioned at the presumptive anterior of the posterior daughter and the posterior of the anterior daughter is constricted to form a new holdfast and the cells are finally separated. Because there are no described methods to synchronize *Stentor* cells, we observed vegetatively growing cultures and isolated cells that presented visible evidence of cell division. Although the earliest stages of division are difficult to identify within a culture we were able to isolate cells from stage 2 all the way through stage 8 (Figure 12). From these data, we were able to determine that Mob1 expands its posterior localization by stage 3 or 4. By stage 5 that expansion begins to focus into a discrete band around the midline and by stage 6 this band spread around the cell, anterior of the oral primordium and is positioned near the presumptive posterior pole of the anterior daughter cell. During stages 7 and 8 this band clearly defined the constriction of the

**Figure 12: Mob1 localizes to the presumptive posterior during cell division.**

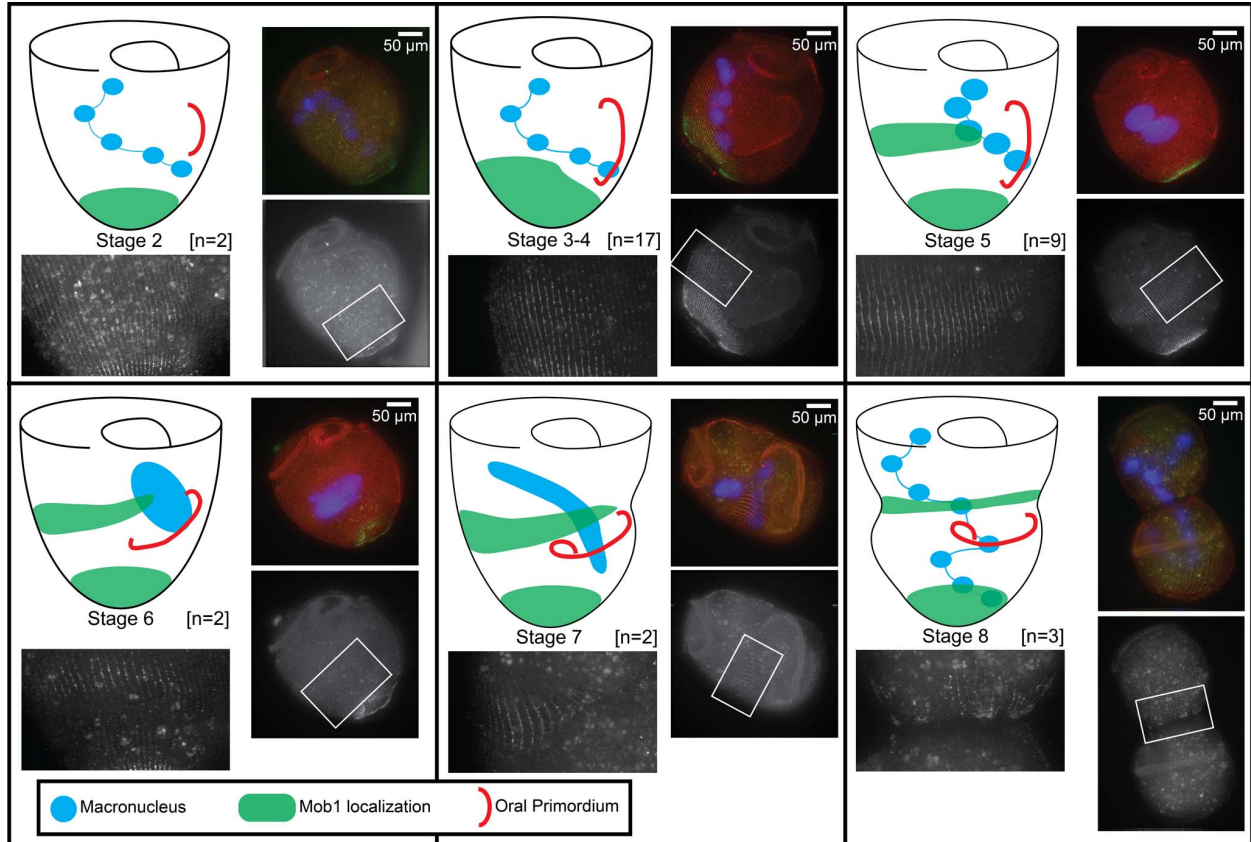


Figure 12. Cartoon showing Mob1 localization next to representative immunofluorescence images for each stage of division. Regions indicated by the white boxes are magnified in the adjacent images to clearly show Mob1 localization. Stage 2 (n=2), Stage 3-4 (n=17), Stage 5 (n=9), Stage 6 (n=2), Stage 7 (n=2) and Stage 8 (n=3) are represented. Mob1 appears to migrate up from the posterior during stages 3-4 and focuses into a band around the midline in stage 5. Through the end of division this band is maintained and forms a clear border between the two daughter cells, which later becomes the posterior end of the anterior daughter cell. High levels of background autofluorescence from *Chlamydomonas* containing food vacuoles is often a problem because cells were fed continuously for this experiment but Mob1 staining can be seen specifically along cortical rows indicated by white arrowheads. The cells imaged in

stage 7 were too large to fit in a single frame and two separate images were taken with identical settings, then manually stitched together using the cortical rows for alignment

newly forming posterior and there was a clear break between the two halves of the dividing cell. Thus, Mob1 appears to localize at the posterior end of the anterior daughter cell prior to completion of cell division.

To determine the function of Mob1 in *Stentor* cells we created an RNAi vector targeting Mob1 sequence. Because of the high sequence similarity among the *Stentor* Mob1 homologs, 85 – 95% identity at the nucleotide level (Figure 13), we expect that any long dsRNA Mob1 construct would target all six Mob1 genes, although we specifically used Mob1a for this study. When aligned pairwise with all other *Stentor* Mob1 homologs, Mob1a shared at least one  $\geq 20$ mer between the sequences for all possible pairs and so it is possible that this single construct would be sufficient for the knockdown of all Mob1 genes. Additionally, RNAi constructs were made specifically targeting Mob1b, c, and d as well and all gave identical results (data not shown). Because the MOB family of proteins has conserved functions in both cell division and morphogenesis we expected phenotypes that would affect cytokinesis and cell polarity [21]. RNAi knockdown of Mob1 in *Stentor* was extremely effective, and resulted in a 30-fold reduction of Mob1a transcript levels compared to the GAPDH control after 4 days of feeding (Figure 14A). This treatment caused dramatic defects in *Stentor* morphology, which progressively worsened as feeding of the RNAi vector continued. After 24-48 hours of RNAi, we observed cells with altered cell proportionality; cells had lost their characteristic “wine-glass” shape and became more cylindrical (Figure 14B, 14C, 15). Mob1 thus appears to play a key role in the regulation of proportional cell shape, the phenomenon first characterized by Morgan in his landmark 1901 paper [9]. Between 48

Figure 13: Sequence alignment of *Stentor* Mob1 genes.

Mob1a	ATGGATAAAGGCTCAGACAAAAACAAGAGTTTCAGGCCGGAAGAAGAGAATGAAAAAGGC	60
Mob1f	ATGGATAAAGGCTCAGACAAAAACAAGAGTTTCAGGCCGGAAGAAGCCAATGAAAAAGGC	60
Mob1b	ATGGATAAAGGCTCCGACAAAAACAAGAGCTTCGGCCCTAAAAAGCCATAGAAAAAGGT	60
Mob1c	ATGGATAAAGGCTCAGACAAAAACAAGAGCTTCAGGCCCTAAAAAGCCATAGAAAAAGGT	60
Mob1d	ATGGATAAAGGCTCAGACAAAAACAAGAGCTTCAGGCCGGAAGAAGCCATAGAAAAAGGT	60
Mob1e	ATGGATAAAGGCTTCGACAAAAACAAGAGCTTCAGGCCGGAAGAAGCCATAGAAAAAGGT	60
	***** ** *	
Mob1a	CAAGCTGGCTACGGATTAAAACAAATAGCTAAATGACCTGGCTCAGGAATCTAGAC	120
Mob1f	CAGCGTGGCTATGGATTAAAACAAATTCGCTAAATGACCTAGCTCAGGAATCTAGAT	120
Mob1b	CAGCGTGGTTATGGATTAAAACAAATCGGAAAAATGACCTGGTTCGGGAATCTAGAC	120
Mob1c	CAGCGTGGTTATGGATTAAAACAAATCGGAAAAATGACCTAGCTCAGGAATCTAGAT	120
Mob1d	CAGCGGGATACGGATTAAACCAAATAGCAAAATGACTTAGGCTCAGGAATCTAGAT	120
Mob1e	CAGCGGGATATGGATTAAACCAAATAGCAAAATGACTTAGGCTCAGGAATCTAGAT	120
	** *	
Mob1a	CTTCGAGTTGAATACCAACAGGTGAAGACTTGAACGAATGGTTGGCAGTGAATACAATC	180
Mob1f	CTTCGAGTTGAATGCCAACAGGTGAAGACTTGAACGAATGGTTGGCAGTGAATACAATC	180
Mob1b	CTAGCAGTAGAGCTTCCAACAGGTGAAGACTTAAACGAATGGTTGCCCTAAATACAATC	180
Mob1c	CTAGCAGTAGAGCTTCCAACAGGTGAAGACTTAAACGAATGGTTGCCCTAAATACAATC	180
Mob1d	CTTGCTGTAGACTACCAACAGGTGAAGACTTAAACGAATGGTTAGCCGTGAATACAATC	180
Mob1e	CTTGCTGTAGAGTTACCAACAGGTGAAGACTTAAACGAATGGTTAGCTGTGAATACAATC	180
	** : * : * : * : *	
Mob1a	GAATTTTAAATGAAATCAACCTCATCTATGGAGCTTCTTGGAGTTCTGCACCTCTGAA	240
Mob1f	GAATTTTAAATGAAATTAACCTCATCTATGGAGCTTCTTGGAGTTCTGCACCTCTGAA	240
Mob1b	GAGTTTACAATGAAATTAACCTTAATCTACGGAGCTTACTTGAAGTTTGTACTCTGAA	240
Mob1c	GAGTTTACAATGAAATTAACCTTAATCTACGGAGCTTACTTGAAGTTTGTACTCTGAA	240
Mob1d	GAGTTTAAAGCAATGAAATTAACCTTAATCTACGGAGCTTACTTGAAGTTTGTACTCTGAA	240
Mob1e	GAGTTTAAATGAAATTAACCTTAATCTACGGAGCTTACTTGAAGTTTGTACTCTGAA	240
	** *	
Mob1a	ACTTGTCTTATATGCTCAGCAGGACCAAAATACGAATATCTTTGGGCTGATGGCAAAAC	300
Mob1f	ACTTGTCTTATATGCTCAGCAGGACCAAAATACGAATATCTTTGGGCTGATGGCAAAAC	300
Mob1b	ACTTGTCTTATATGCTCAGCAGGCTCCTAAATAGATATTTATGGGCTGATGGCAAAAC	300
Mob1c	ACTTGTCTTATATGCTCAGCAGGCTCCTAAATAGATATTTATGGGCTGATGGCAAAAC	300
Mob1d	ACTTGTCTTATATGCTCAGCAGGCTCCTAAATAGATATTTATGGGCTGATGGCAAAAC	300
Mob1e	ACATGTCTTATATGCTCAGCAGGCTCCTAAATAGATATTTATGGGCTGATGGCAAAAC	300
	** : * : * : * : *	
Mob1a	ATTAAACTCCTTTAAAGTTTCTGCATCAGAGTATATTGATTTCTCATGACCTGGGTA	360
Mob1f	ATTAAACTCCTTTAAAGTTTCTGCATCAGAGTATATTGATTTCTCATGACCTGGGTA	360
Mob1b	ATAAACACCACTTAAAGTCTCTGCATCAGAGTATATTGACTTTTAAAGACTGGGTA	360
Mob1c	ATAAACACCACTTAAAGTCTCTGCATCAGAGTATATTGACTTTTAAAGACTGGGTA	360
Mob1d	ATCAAACTCCTTTAAAGTCTCTGCATCAGAGTATATTGATTTCTCATGACCTGGGTT	360
Mob1e	ATAAACACCCCTTTAAAGTTTCTGCTTCAGATATATTGATTTCTCATGACCTGGGTT	360
	** *	
Mob1a	GAAAGCAATTGAATAATGAATCCTTGTTCCTACGCAATAGGAGTAGCTTTTCTAAG	420
Mob1f	GAAAGCAATTGAATAATGAATCCTTGTTCCTACGCAATAGGAGTAGCTTTTCTAAG	420
Mob1b	GAAAGCAATTGAATAATGAATCCTTGTTCCTACTCAAAATGGGTATACCAATTTCTAAG	420
Mob1c	GAAAGCAATTGAATAATGAATCCTTGTTCCTACTCAGATGGAGTCCAATTTCTAAG	420
Mob1d	GAAAGCACTTAAATAGAGCTTTGTTCCTACTCAAAATGGAGTCCAATTTCTAAG	420
Mob1e	GAAAGCAGCTTAAATAGAGCTTTGTTCCTACTCAAAATGGAGTCCAATTTCTAAG	420
	***** ** *	
Mob1a	AACTTCCTCTCAGCAATAAAGTGATTTTAAAGAGCTTTAGAGTTTATGGCATATA	480
Mob1f	AACTTCCTCTCAGCAATAAAGTGATTTTAAAGAGCTTTAGAGTTTATGGCATATA	480
Mob1b	AACTTCCTCTCAGCAATAAAGTGATTTTAAAGAGCTTTAGAGTTTATGGCATATA	480
Mob1c	AACTTCCTCTCAGCAATAAAGTGATTTTAAAGAGCTTTAGAGTTTATGGCATATA	480
Mob1d	AACTTCCTCTCAACAAATTAAGGTATTTTAAAGAGCTTTAGAGTTTATGGCATATA	480
Mob1e	AACTTCCTCTCAACAAATTAAGGTATTTTAAAGAGCTTTAGAGTTTATGGCATATA	480
	***** ** *	
Mob1a	TATCATACGCAATTTTACGATATATGAGTTTGGATGGAATATCATCTAAACACTTGT	540
Mob1f	TATCATACGCAATTTTACGATATATGAGTTTGGATGGAATATCATCTAAACACTTGT	540
Mob1b	TATCATACGCAATTTTACGATATATGAGTTTGGATGGAATATCATCTAAACACTTGT	540
Mob1c	TATCATACGCAATTTTACGATATATGAGTTTGGATGGAATATCATCTAAACACTTGT	540
Mob1d	TATCATACGCAATTTTACGATATATGAGTTTGGATGGAATATCATCTAAACACTTGT	540
Mob1e	TATCATACGCAATTTTACGATATATGAGTTTGGATGGAATATCATCTAAACACTTGT	540
	** *	
Mob1a	TTCAAGCATTATATATTTTTATAGACAGATTCAAACTAGTCGACCAAAAAGAAATAGCT	600
Mob1f	TTCAAGCATTATATATTTTTATAGACAGATTCAAACTAGTCGACCAAAAAGAAATAGCT	600
Mob1b	TTCAAGCATTATATATTTTTATAGACAGGTTTAAACTTGTAGATCAGAAAGAACTGGCC	600
Mob1c	TTCAAGCATTATATATTTTTATAGACAGGTTTAAACTTGTAGATCAGAAAGAACTGGCC	600
Mob1d	TTCAAGCATTATATATTTTTATAGACAGGTTTAAACTTGTAGATCAGAAAGAACTGGCC	600
Mob1e	TTTAAACATTATATATTTTTATAGATGATTTAAACTTGTAGATCAGAAAGAACTGGCC	600
	** *	
Mob1a	CCTCTTCGAGCTATACAGCAGTTTCGAGAACGAGGTAGGGAAGAATGGAACGAGAA	660
Mob1f	CCACTTCGAGCTATACAGCAGTTTCGAGAACGAGGTAGGGAAGAATGGAACGAGAA	660
Mob1b	CCACTTCGAGCTATACACAGTTTAGAGAAAGAGGTAGGGAAGAGATGGAAGGGAG	660
Mob1c	CCTCTTCGAGCTATACAGCAGTTTAGAGAAAGAGGTAGGGAAGAATGGAACGAGAA	660
Mob1d	CCTCTTCGAGCTATACAGCAGTTTAGAGAAAGAGGTAGGGAAGAATGGAAGGGAG	660
Mob1e	CCTCTTCGAGCTATACACAGTTTAGAGAAAGAGGTAGGGAAGAATGGAACGAGAA	660
	** : * : * : * : *	
Mob1a	GCTTCGGTAACTAA----- 675	
Mob1f	GCTTCGGTAACTGA----- 675	
Mob1b	GCTTCGGTAACTGA----- 675	
Mob1c	GCTTCGGTAACTGA----- 675	
Mob1d	GCTTCGGAGGTAGAGGATA 681	
Mob1e	GCTTCGTA----- 669	
	** *	

Figure 13. Clustal Omega alignment of all Stentor Mob1 nucleotide sequences was performed using default settings. Using Mob1a as a reference point for pairwise alignments to all other Mob1 homologs, there is at least one 20mer predicted to be shared between each of the pairs.



**Figure 14: *Mob1(RNAi)* cells lose proper cell proportions and body axes.**

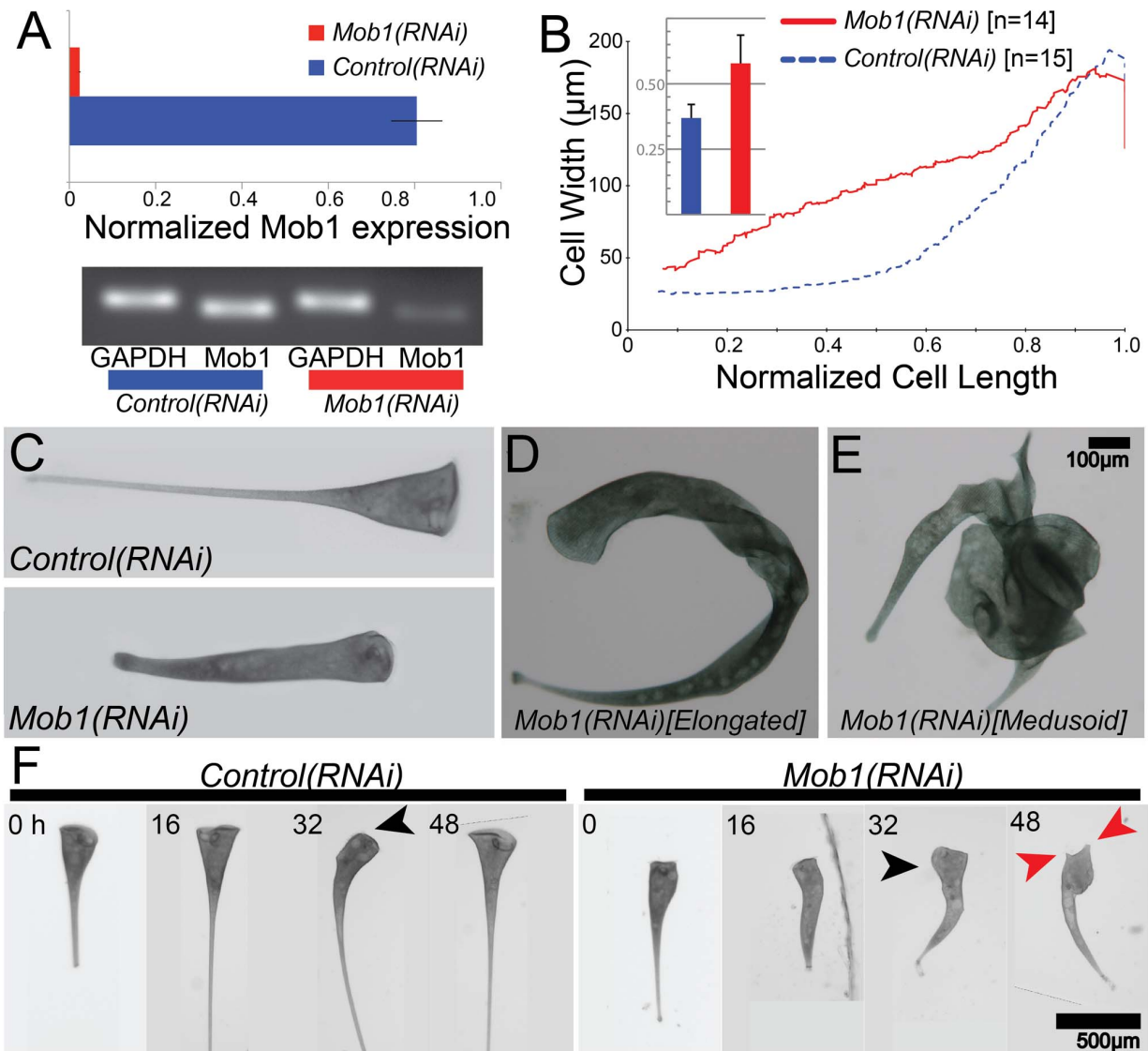


Figure 14. **(A)** qRT-PCR data showing relative expression of *Mob1* normalized to *GAPDH* expression in control and *Mob1(RNAi)* cells. **(B)** Quantitative analysis of the proportionality defect plotted as a graph of cell width vs. normalized cell length for *control(RNAi)* (blue, n=3) and *Mob1(RNAi)* (red, n=4) cells. Data for each line represents a moving average of all samples with a window size of 2n. These measurements were used to compute a shape factor as described in Materials and

Methods and graphed in the inset bar graph. The shape factor describes deviation from a shape having perfect straight lines on the cell edge. Data in the inset show an increase in shape factor from  $0.37 \pm 0.052$  (n=15) in control cells to  $0.58 \pm 0.108$  (n=14) in *Mob1(RNAi)* cells, a highly significant increase ( $p=1.8 \times 10^{-6}$ ). **(C)** Control cell's canonical shape as compared to a *Mob1(RNAi)* cell fed the RNAi vector for 3 days, showing altered cell proportionality. **(D, E)** Brightfield image of an elongated (D) and medusoid (E) cell. **(F)** Selected images from a time-course. *Control(RNAi)* and *Mob1(RNAi)* cells were isolated after 2 days of feeding and imaged every 2 hours for an additional 52 hours. Spontaneous reorganization of the OA (black arrows) occurred prior to the multipolar phenotype (red arrows) in *Mob1(RNAi)* cells.

**Figure 15: Cell shape analysis of control and *Mob1(RNAi)* cells shows a loss of normal proportions.**

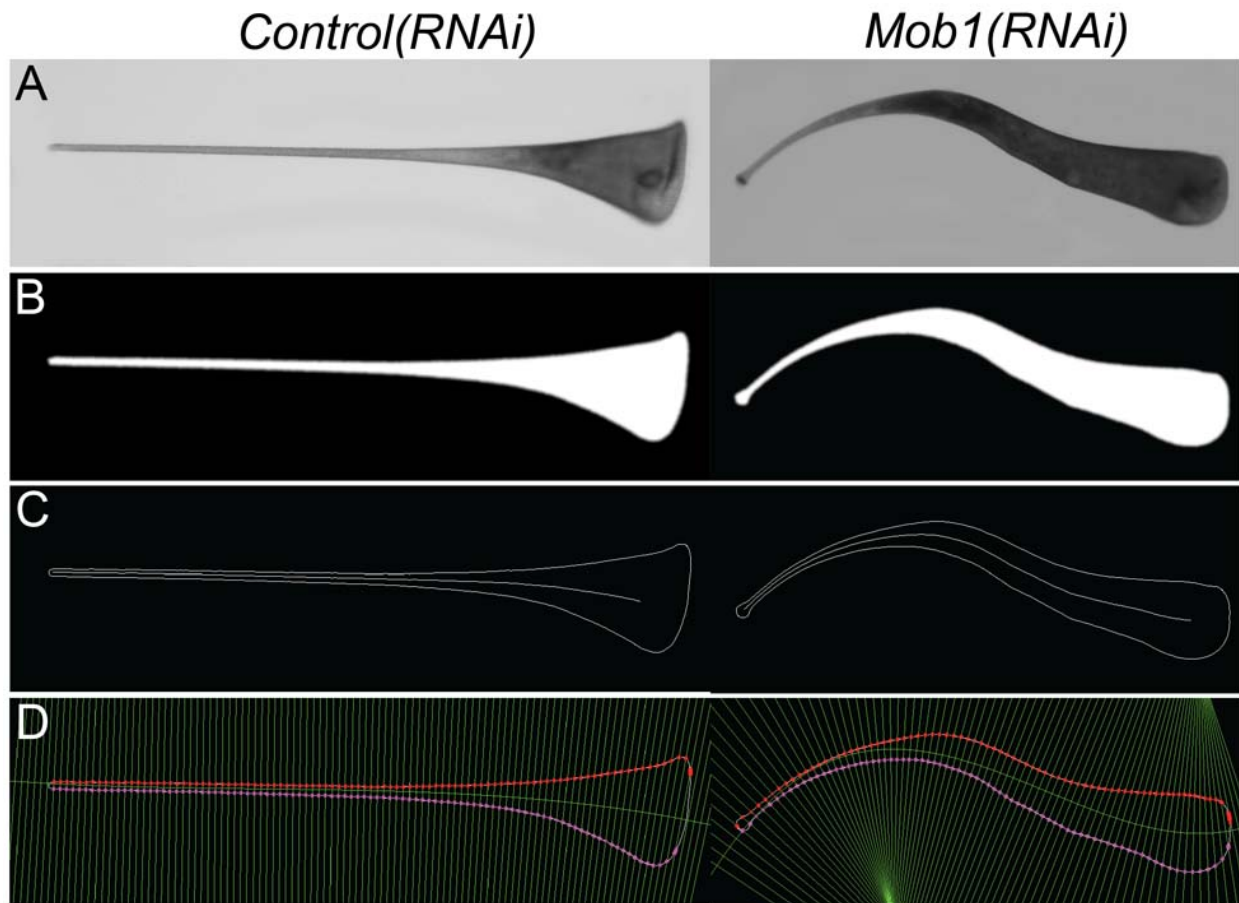


Figure 15. **(A)** Brightfield images used as the input for the cell shape analysis process. **(B)** Thresholded black and white images are then further processed by two rounds of the smoothing function in ImageJ. **(C)** The cell outline was detected using the black and white image as an input for our MatLab program, and the image was skeletonized to find the midline. **(D)** The cell midline is then fit to a curve and perpendicular lines are drawn. The intersection of these perpendicular lines with the cell outlines (red and pink X's) are then used to determine the cell widths.

and 96 hours of Mob1 knockdown, cells displayed further morphological abnormalities that could be separated into two categories. The first consisted of cells that were highly elongated and curved, apparently a result of a deformed cortex, which caused the cells to twist (Figure 14D). The other class of defects consisted of multipolar (medusoid) cells with multiple OA regeneration bands and ectopic tails, growing from the cell body, that were often functional posteriors (Figure 14E). These morphological effects were not observed with RNAi targeting any other genes we tested, suggesting they are specific to the Mob1 knockdown. Identical phenotypes were observed when either half of the gene was targeted separately (Figure 16). In addition to these morphological defects, Mob1 knockdown cells show clear defects in cytokinesis (Figure 17), comparable to those observed in *Tetrahymena*, although cell division was rare and seen in less than 5% of *Mob1(RNAi)* cells over a 5 day period which is typical for *Stentor* in our growth conditions [22].

Some of the more severely affected medusoid cells were so abnormally shaped that it was impossible to define what had happened to the cells from only a single time-point, raising the possibility that multiple failed attempts at cell division might have played a role in development of the phenotype. To obtain a clear idea of the development of these phenotypes we imaged individual cells every 2 hours after feeding them the RNAi vector for 48 hours. We observed that all cells went through similar stages of aberrant morphogenesis (Figure 14F, 18), initially losing their canonical “wine-glass” proportions and elongating slightly relatively early in the time-course (Figure 14F, 16h), and eventually converting to the medusoid form. During the evolution of the *Mob1(RNAi)* phenotype, cells underwent a round of spontaneous regeneration of

**Figure 16: The Mob1(RNAi) phenotypes are specific to the Mob1 sequence.**

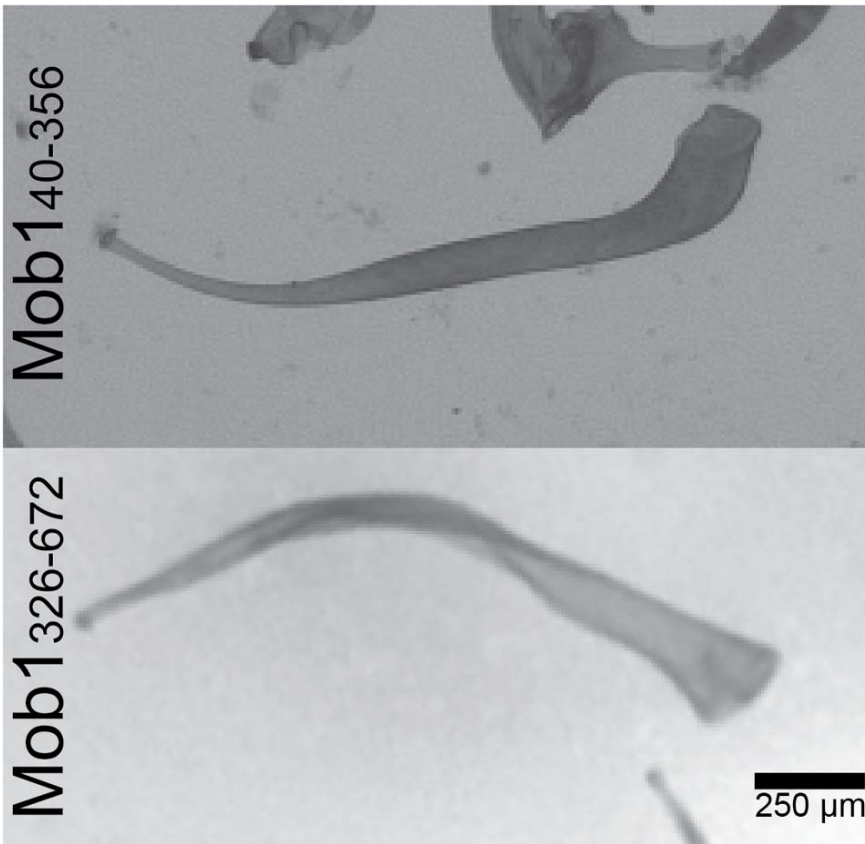
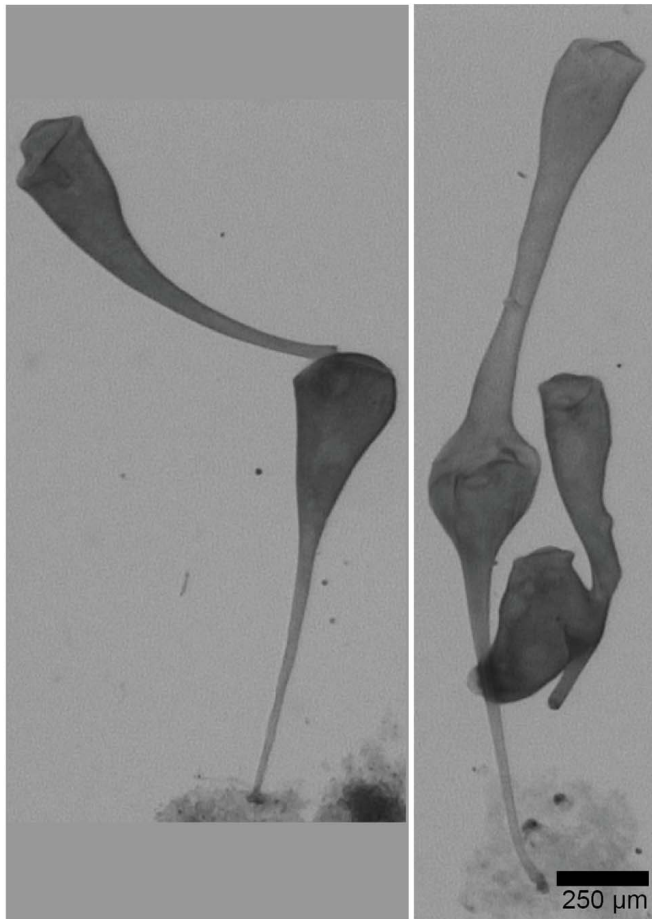


Figure 16. (A) Brightfield images of split *Mob1*(RNAi) constructs. Targeting either the first half (40-356) or the second half (326-672) yield the elongated cell phenotype after 5 days of feeding.

**Figure 17: Mob1(RNAi) disrupts normal cell division.**



*Control(RNAi)*

*Mob1  
(RNAi)*

Figure 17. Brightfield images of control and *Mob1(RNAi)* cells at the end of cell division. Control cells separate properly at the end of cytokinesis whereas the *Mob1(RNAi)* cells remain attached.

Figure 18: Progression of the Mob1(RNAi) phenotype.

## Progression of *Mob1(RNAi)* Phenotype

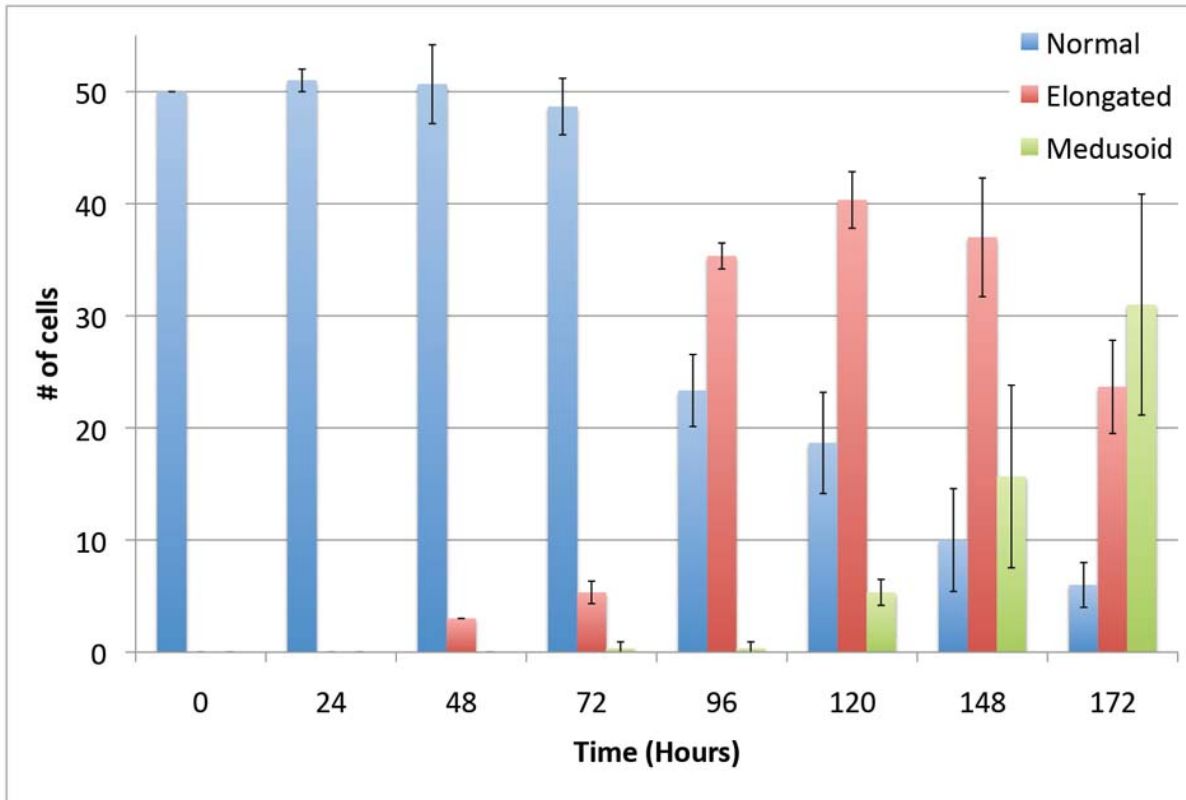


Figure 18. Graph displaying data from a population of 50 cells fed the Mob1 RNAi vector over the course of 172 hours. Cells were visually scored for phenotypes once per day for either a normal, elongated, or medusoid appearance. Any increase in the total number of cells above 50 is the result of cell division during the course of the experiment. This experiment was done in triplicate, and the error bars represent the standard deviations for each time point.

the oral apparatus (OA). This is a normal process in *Stentor* and does not normally result in aberrant morphogenesis; but in *Mob1(RNAi)* cells, spontaneous OA regeneration was immediately followed by off-axis growth, i.e. the extension of a new posterior pole along an axis different from the previously existing anterior-posterior axis, indicating that this process might trigger the development of further defects (Figure 14F, 32 h). The cell cycle of *Stentor* is between 96 and 120 hours in our growth conditions and, consistent with this long duration, we found that no cells initiated cell division during the 52-hour observation period, making it unlikely that the observed morphological defects could be products of failed cytokineses (n=20). These data suggest that Mob1 is required for OA localization and for the proper regulation of posterior structures; and in the absence of Mob1, posterior growth becomes unregulated. However, our results also imply that regeneration of the OA might be triggering the development of more severe defects and a switch from disproportioned and elongated bipolar cells to multipolar cells.

Interestingly, when we localized residual Mob1 protein at different stages in *Mob1(RNAi)* cells (Figure 19), we noted that Mob1 protein is first lost from more anterior regions (Figure 19B), and only by the medusoid stage is Mob1 staining almost completely absent (Figure 19C). This raises the possibility that differentially localized Mob1 is performing different functions in *Stentor*, and its loss in these specific locations triggers the development of different phenotypes.

We next hypothesized that if different populations of Mob1 perform different functions in the cell, we would be able to determine these functional differences using microsurgery to remove specific regions of the cell containing Mob1. In the case of a



Figure 19: Presence of residual Mob1 protein in *Mob1(RNAi)* cells.

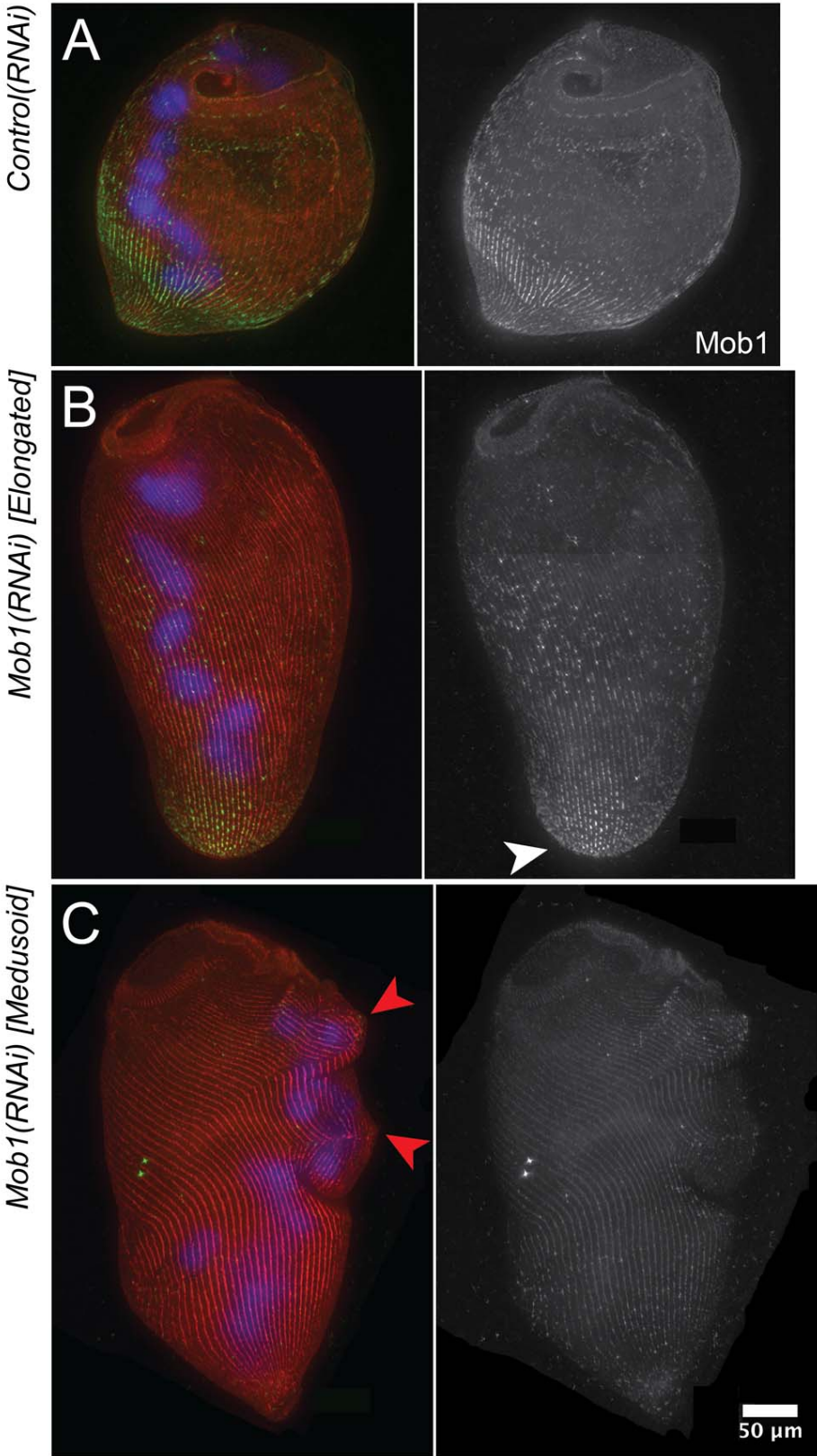


Figure 19. **(A)** Immunofluorescence images of stained *control(RNAi)* cells showing Mob1 localization (green, anti-Mob1), macronucleus (blue, DAPI) and cortical rows (red, stentorin-autofluorescence). **(B, C)** Immunofluorescence images of a stained elongated (B) and medusoid (C) *Mob1(RNAi)* cells; Mob1 (green, anti-Mob1), macronucleus (blue, DAPI), and cortical rows (red, stentorin autofluorescence), compare to (A). Cortical aberrations are seen in the cortical rows (red arrows). Both the elongated and medusoid cells were too large to fit in a single frame and two separate images were taken with identical settings, then manually stitched together using the cortical rows for alignment (seam is indicated by a dashed yellow line).

simple bisection, the anterior fragment of the cell would lack the posterior population of Mob1 and need to regenerate posterior structures, whereas the posterior fragment would lack the anterior population of Mob1 and need to regenerate a new OA and anterior (Figure 4). Morphologically normal cells, taken after 72 hours of feeding the Mob1 RNAi vector, were bisected and those fragments were observed every two hours. Compared to control cells (Figure 20A), *Mob1(RNAi)* cell fragments grow ectopic tails resembling normal posterior structures (Figure 20B). Anterior fragments maintained the original OA, and only grew ectopic tails adjacent to the previous posterior structures, which would suggest that the OA has some control over posterior growth. Conversely, posterior fragments failed to properly localize their regenerating OA, which remained on the dorsal side of the cell, and resulted in cells that were able to grow new posterior structures at the anterior end. These results show that Mob1 is not required to initiate regeneration, although once initiated neither the anterior nor posterior halves properly regenerated the OA or the holdfast. Furthermore, this suggests that Mob1 plays a key role in defining polarity and regulating polarized cell growth during normal development as well as regeneration.

Interestingly, 10% of cells were only mildly affected and successfully regenerated their missing structures (holdfast and OA). However, they still lost normal cell proportions, indicating that the RNAi had occurred in these cells (n=20, Figure 20C). We hypothesize that these cells represent incomplete knockdown of Mob1, and that cell proportionality is more sensitive to Mob1 depletion than OA and posterior pole formation. The fact that proportionality defects can occur without inducing regeneration suggests that these two phenotypes are functionally separable.

**Figure 20: Morgan revisited: regeneration of proportionate structures in *Stentor* requires Mob1 protein.**

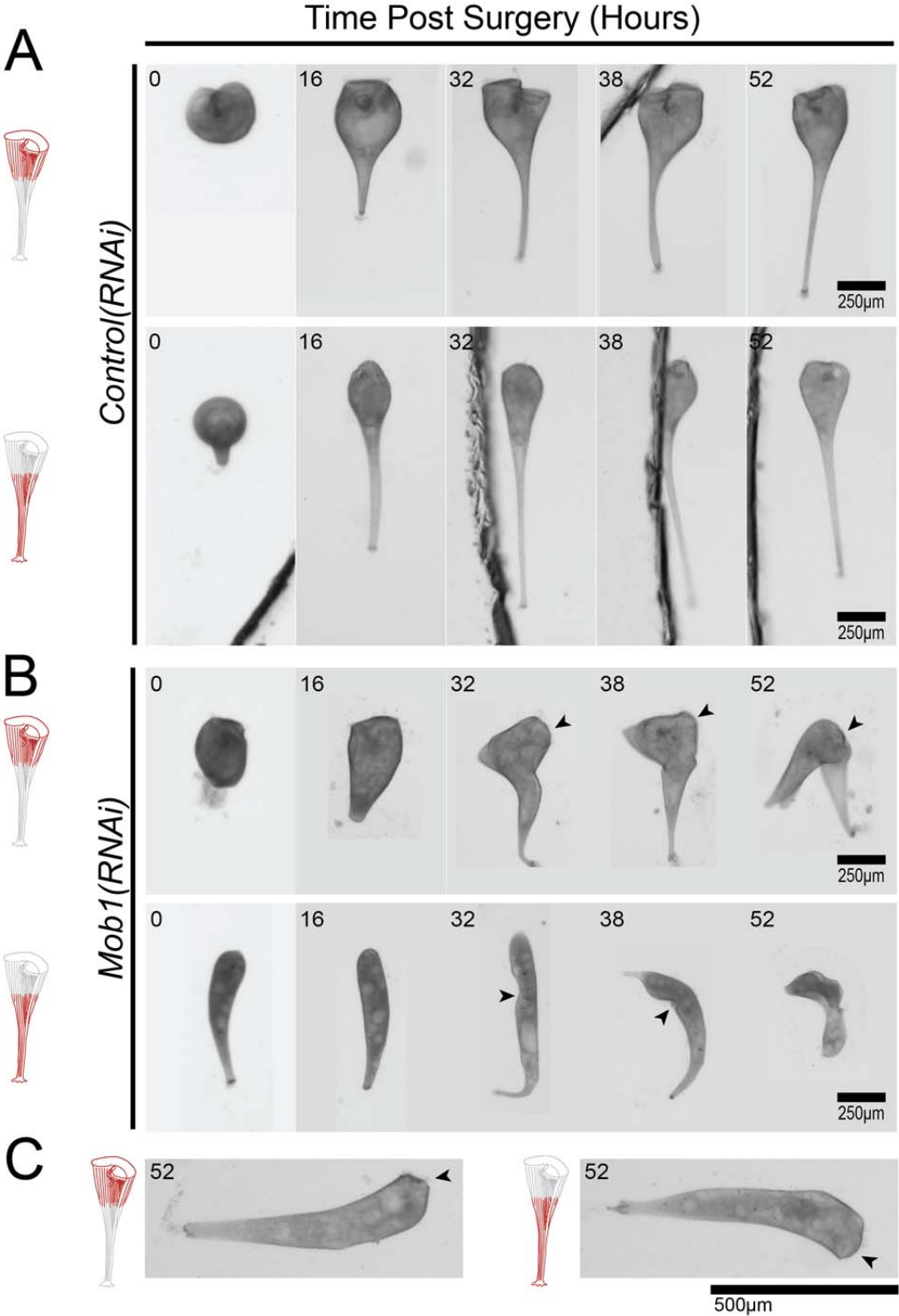


Figure 20. **(A-C)** Observed fragments of cells are shown in red, and OAs are indicated with black arrowheads where they are difficult to identify. **(A)** Regeneration of both anterior and posterior fragments of control cells after surgical bisection. **(B)** Regeneration of both anterior and posterior fragments of bisected *Mob1(RNAi)* cells after 3 days of feeding on the RNAi vector. **(C)** Anterior and posterior *Mob1(RNAi)* cell fragments regenerated OA/holdfast properly in 10% of cells but failed to re-establish normal cell proportions (n=20).

A challenge for using RNAi to study development is that phenotypes can take time to fully develop because protein turnover takes a longer time than transcript knockdown. Such a lag between message depletion and protein depletion is a universal feature of RNAi in all organisms and simply reflects the greater stability of protein compared to mRNA. In the case of *Stentor*, Mob1 knockdown cells observed 48 hours into the RNAi timecourse still showed normal morphology and were able to fully regenerate after bisection, to an extent comparable to *control(RNAi)* cells (Figure 21A), despite the fact that mRNA levels were dramatically reduced relative to controls. This phenotypic lag relative to the timing of mRNA knockdown along with immunofluorescence data that clearly shows the presence of Mob1 protein in the posterior even in elongated cells (Figure 19B) suggested that there could still be a sufficient amount of Mob1 protein to function during regeneration. In most systems there is no way to bypass this phenotypic lag and one must simply accept it as a caveat for RNAi experiments, but in our case the ease of *Stentor* manipulation provides a way to speed up the development of an RNAi phenotype by physically removing the parts of a cell where the target protein resides. To this end, we surgically removed the head and the tail, which are the portions of the cell where the majority of Mob1 protein is localized, after inducing Mob1 knockdown by RNAi. If the phenotypic lag was due to retained protein in these regions, this surgical operation should reduce the lag between mRNA knockdown and development of morphological phenotypes. In *Control(RNAi)* cells, removal of both the head and tail structures yielded morphologically normal cells after 24 hours (Figure 21B, top), with Mob1 signal returning as early as 3 hours post-surgery as observed by immunofluorescence (Figure 22). However, when both the heads and tails were

**Figure 21: Residual Mob1 in the anterior and posterior can be surgically removed.**

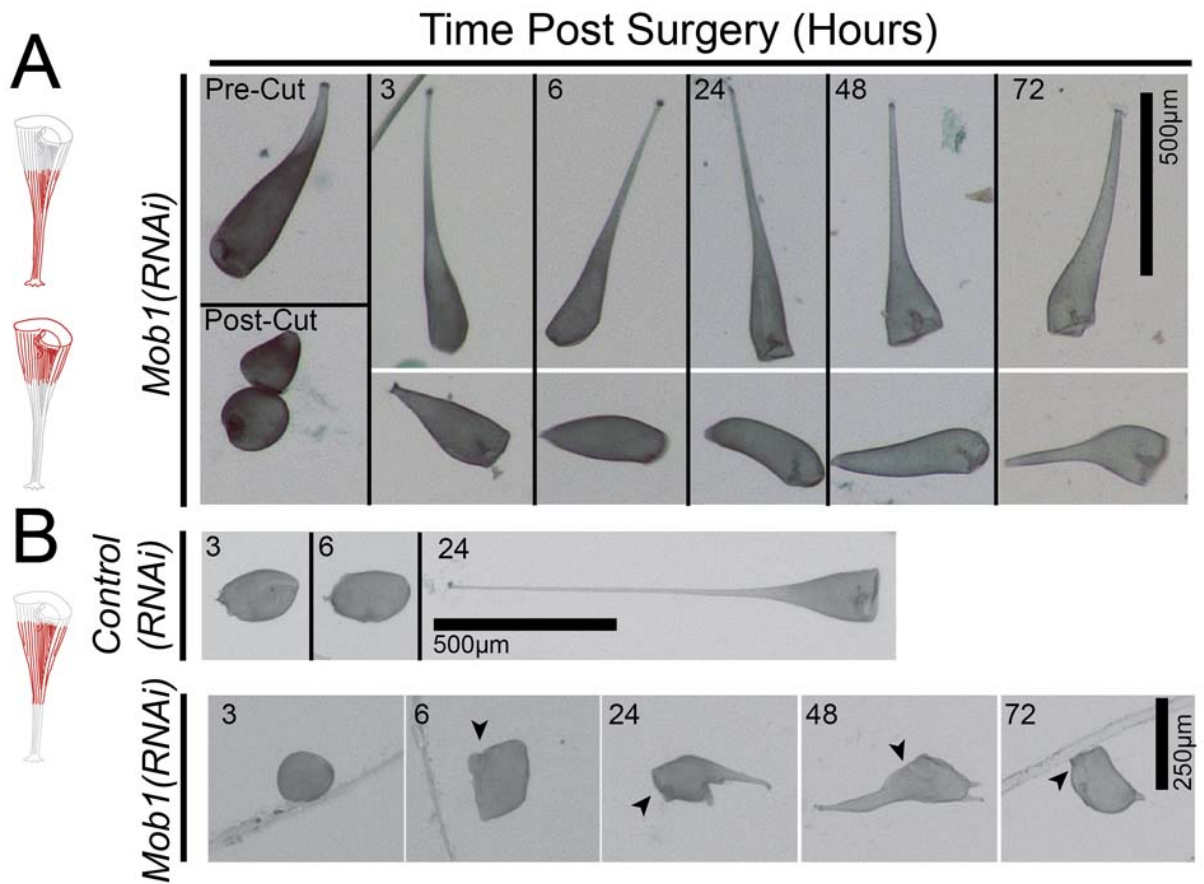


Figure 21. **(A, B)** Observed fragments of cells are shown in red, and OAs are indicated with black arrowheads where they are difficult to identify. **(A)** *Mob1(RNAi)* cells that are bisected only 2 days after feeding the RNAi vector are capable of normal regeneration. **(B)** *Control(RNAi)* and *Mob1(RNAi)* cells had their anterior and posterior regions excised to remove regions of the cell where Mob1 localizes. Only removal of both Mob1-containing poles in *Mob1(RNAi)* cells prevented regeneration at this early stage of the RNAi time-course.

**Figure 22: Reappearance of Mob1 in regenerating cells.**

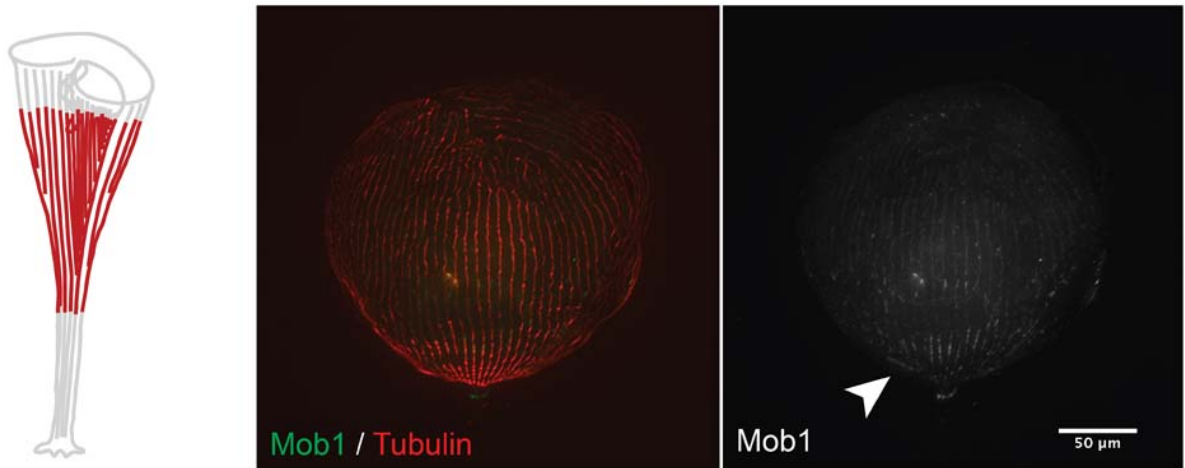


Figure 22. Immunofluorescence image showing a cell 3 hours after the surgical removal of both the anterior and posterior. Mob1 (green, anti-Mob1) can be seen in the posterior of the cell, indicated by the white arrowhead.



removed from morphologically normal *Mob1(RNAi)* cells at an early stage of knockdown when cells still showed normal morphology, they developed phenotypes similar to those seen at much later stages of *Mob1* knockdown (Figure 8B, bottom). The result that surgically accelerated removal of *Mob1* proteins reduces the lag between gene knockdown and development of morphological phenotypes supports the idea that *Mob1* protein functions globally in establishing both anterior and posterior polarity in *Stentor*.

The ability to perform RNAi in *Stentor* to manipulate genes of interest, such as we have done with *Mob1*, will pave the way for many future studies to unravel the mechanism of single celled pattern formation and regeneration. Although the standard drawbacks of RNAi still apply to *Stentor*, namely the cell-to-cell variability in the level of knockdown and phenotypic lag due to target protein stability, *Stentor* provides unique methods for addressing these issues because manipulating individual cells is trivial and surgical removal of the protein pool is possible, at least when the target protein is concentrated in a specific region of the cell.

These results, to our knowledge, represent the first molecular analysis of regeneration in *Stentor* to be reported and build on observations of proportional regeneration first made by Morgan over 100 years ago. The kinase co-activator *Mob1* is clearly localized to the posterior in vegetative cells. At distinct stages during cell division *Mob1* is found to first expand toward the anterior, where it is later focused into a discrete band around the midline of the cell. Toward the end of division it creates a clear boundary between the daughter cells, where it localizes to the newly forming posterior of the anterior daughter cell. Localization of *Mob1* to the midline of dividing cells is not unique to *Stentor* and is comparable to observations of *Mob1* in a variety of other

organisms, including *Tetrahymena* [22], Alfalfa [31], and budding yeast [32], although it is interesting to note that Mob1 is clearly asymmetrically localized to the anterior daughter at the midline of both *Stentor* and *Tetrahymena* during division.

Loss of Mob1 due to RNAi knockdown results in a loss of normal proportions, apparent uncontrolled cell growth, and cytokinesis defects. When considering these data alongside the data from *Tetrahymena* it certainly suggests that the single ciliate MOB family member might share the more specialized functions of the multiple MOB family members in other organisms, which has also been suggested by Tavares et al [22]. Although it is still unknown if any of the functional interactions of the MOB family are also conserved in ciliates, such as specific interactions with NDR kinases and STE-like kinases, we hope to address these questions in the future with the advent of a more complete *Stentor* genome.

From these data we can conclude that Mob1 is essential for maintenance and regeneration of cell polarity and proper cell proportions. We also show that RNAi by feeding can now be used as a routine tool to study morphogenesis and regeneration at the level of single cells in *Stentor*. There are likely to be many localized pattern regulatory proteins in addition to Mob1 that control development in *Stentor*, and Mob1 will serve as a model for their study. With this remarkable single cell system we have opened the doors to studying the molecular mechanisms of regeneration at a resolution impossible to attain in other regenerative models. Moving forward we hope to develop more ways to manipulate *Stentor* and further investigate the role of Mob1, and its associated pathways, in order to expand our knowledge of cell polarity, regeneration, and morphogenesis.

## Chapter 4: Extent of macronuclear amplification

Ciliates are binucleate organisms and contain both a germline micronucleus (MIC) as well as a somatic macronucleus (MAC). The MIC is diploid and transcriptionally silent, and relative to the MAC it contains fewer chromosomes. The MAC is transcriptionally active and represents a differentiated MIC, where as much as 80% of the MIC DNA content is removed through a process of programmed DNA elimination which also results in fragmentation of the MIC chromosomes. The final step of MAC differentiation is the amplification of the remaining DNA sequences, resulting in a highly polyploid MAC.

The level of amplification/polyploidy varies greatly between ciliate organisms, although the mechanism that determines the MAC ploidy of an organism remains unknown and there are currently no known estimates of MAC ploidy in *Stentor coeruleus*. Based on the numbers determined from other organisms, it would seem that MAC ploidy roughly scales with cell size, but no direct connection between cell size and ploidy has been demonstrated. Interestingly, Heterotrichs are among the largest ciliates with *Stentor coeruleus* being one of the largest Heterotrichs, so it will be interesting to determine the extent of MAC amplification in this organism. Because the only MAC ploidy estimate from a Heterotrich is *Spirostomum* [33], I expect that it might be the closest reference point for *Stentor coeruleus* and so predict that cells will contain 13,000+ copies of the MAC genome. In order to determine the exact copy number in *Stentor coeruleus* I used digital droplet PCR on whole cell preparations of individual cells.

Digital droplet PCR is an excellent tool for determining copy number variation in *Stentor* with the resolution of individual cells. Briefly, ddPCR relies on splitting the bulk PCR mixture into ~20,000 droplets, and then assaying individual droplets for the presence of a PCR product using specific fluorescent probes and then calculates the starting concentration as copies per  $\mu\text{L}$  (Figure 23). From this, I have determined that the average MAC copy number in *Stentor* cells varies greatly. Data from 14 individual cells suggests that average gene copy number in *Stentor* is 56,630 with a standard deviation of 17,630. Data was collected for three different genes on three different contigs, and each was normalized to a reference gene from the same starting sample (Figure 24A). To make sure that there wasn't a bias based on the size of the contig chosen, I used three contigs of different sizes: 233, 140, and 46 kb.

The level of variation from cell to cell was surprising as it was almost 33% of the average copy number. In order to better understand the source of this variation I also measured the size of each cell and determined the total volume of the MAC. When plotted against copy number, I found that ploidy roughly scales with both cell size and MAC volume (Figure 24B). This isn't all that surprising as it is easy to imagine that larger nuclei contain more DNA and thus more copies of the genome, especially considering De Terra's findings that DNA replication occurs nearly continuously throughout the cell cycle [34]. This would also explain the correlation of copy number with cell size, as cells grow throughout the cell cycle they are also constantly replicating their DNA. This constant increase in DNA content as the cell grows in size likely represents a mechanism to cope with an increasing need for protein production.

Figure 23: Using ddPCR to determine copy number in *Stentor*.

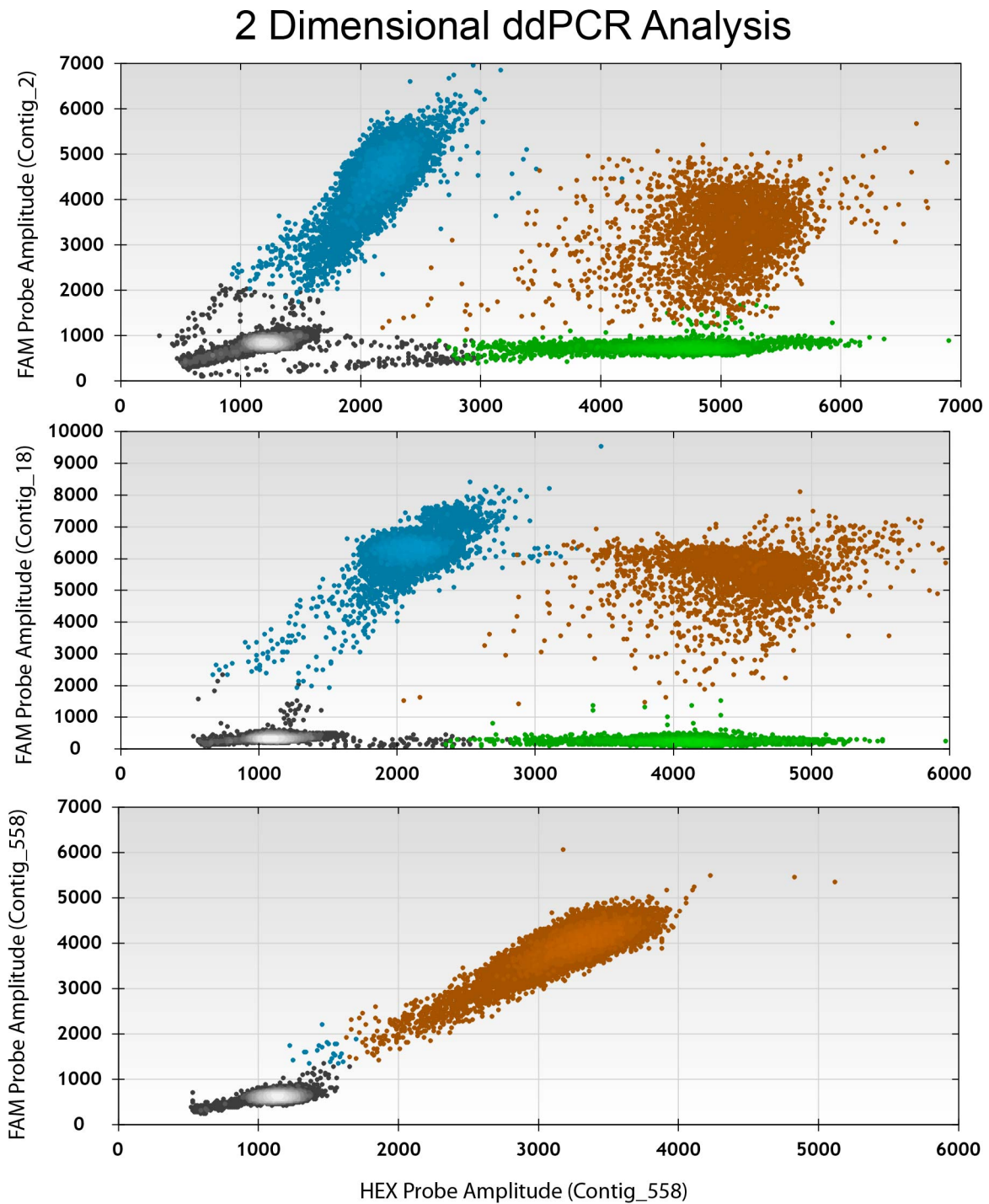


Figure 23. Raw data from ddPCR experiments showing the fluorescent intensity of individual droplets. Here is shown data from contig\_2, contig\_18, or contig\_558 (using

the FAM probe) all compared directly to contig\_558 (using the HEX probe). Droplets containing only product detected by the FAM probe (Blue), HEX probe (Green) or double positive (Orange) are shown. As an internal control, you can see that all droplets from the contig\_558 vs. contig\_558 plot are double positive. Graphs were generated using the Quantasoft software (BioRad).

**Figure 24: Gene copy number in *Stentor*.**

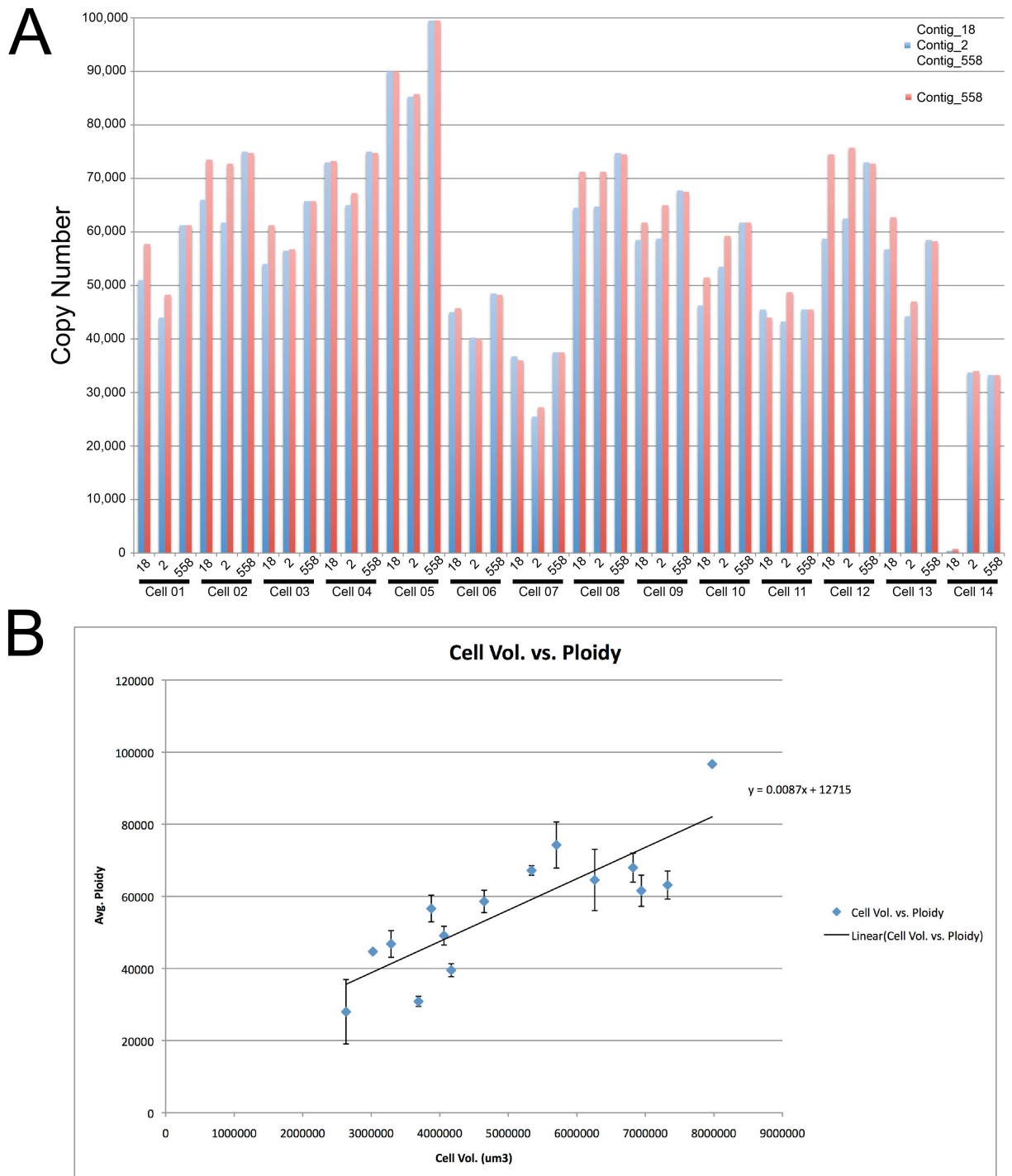


Figure 24. **(A)** Calculations were performed on the raw data to convert copies/ $\mu$ L into total copies per cell as described in the “Materials and Methods” chapter. Samples from

each of 14 cells are shown with their corresponding contig\_558 reference data. These values were then normalized and averaged to obtain an average copy number of 56,630. Importantly, values from different contigs yield similar although not identical values. **(B)** Graph of recorded cell volumes plotted against their average gene ploidy. There is a clear trend between cell size and gene copy number.



Most surprising was the extent of amplification of the rDNA chromosome. In ciliates the rDNA chromosome is kept extra-chromosomally and maintained at extremely high copy number relative to even the level of amplification for normal genes in the MAC. For example, in *Paramecium* the average MAC copy number for somatic genes is 1000 whereas the rDNA chromosome is present at ~20,000 copies [35]. In *Stentor*, the 18s rDNA sequence was found on its own contig in the genome assembly and its copy number was determined using ddPCR (Figure 25). The 18s rDNA chromosome is present between 10 - 30 fold higher levels relative to the other three genomic loci, with an average copy number of 1,117,308 +/- 459,853. Along with the gene copy number, this is the highest copy number in ciliates that I am aware of and likely reflects the immense size of *Stentor coeruleus*. More studies will have to be done in order to better understand the relationship between cell size and gene copy number in *Stentor* and how that might also apply to other ciliates or non-ciliate organisms but these initial results are certainly interesting.

**Figure 25: rDNA copy number scales with cell size.**

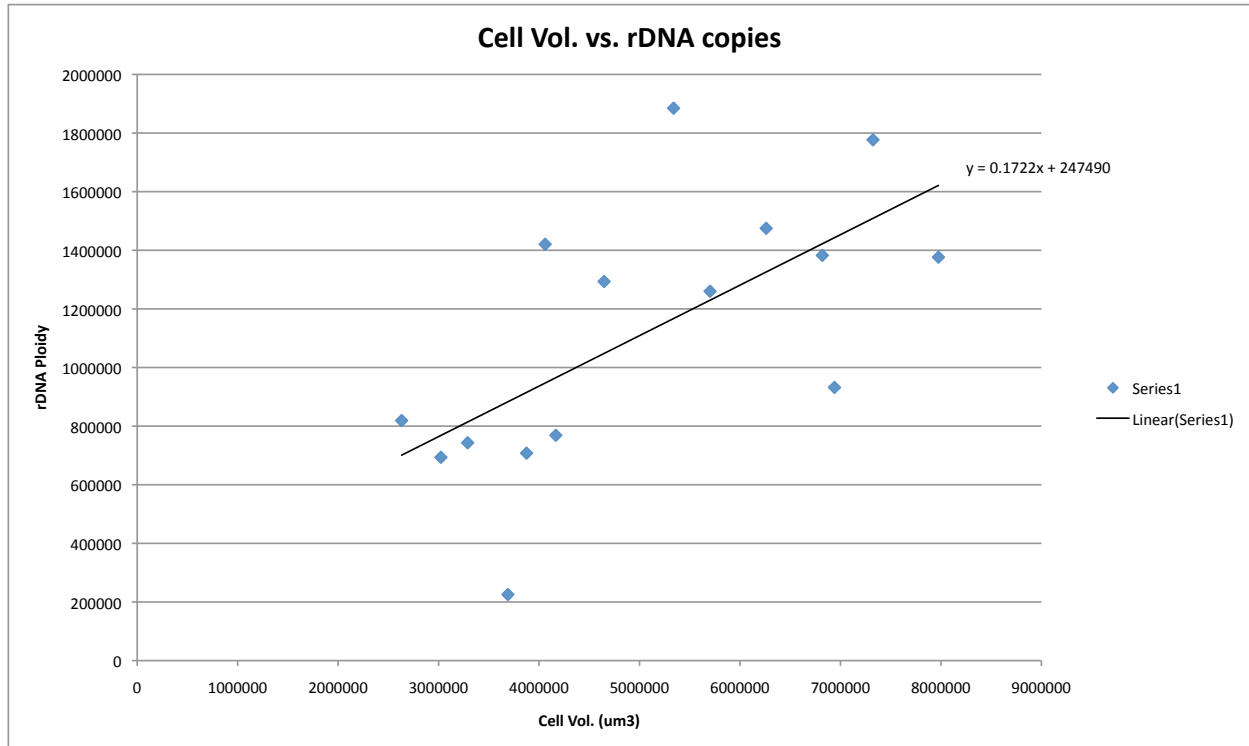


Figure 25. Graph of cell volume vs. rDNA copy number. Samples had to be diluted an extra 1:100 in order to operate within the dynamic range of the ddPCR machine. I again used contig\_558 as a reference for normalization and compared this data to the data from Figure 24 and all values were internally consistent. rDNA copy number is extremely amplified in *Stentor coeruleus* and also increases with cell volume.

## **Chapter 5: Isolation of five *Stentor* species from two ponds near Woods Hole Marine Biological Laboratory.**

There is amazing diversity within the *Stentor* genus, and various species have vastly different shapes, sizes, behaviors, and colors. Additionally, many of these species are ubiquitous and can be found in freshwater lakes, ponds, and slow moving streams around the world. Many species have been named in the literature, however most of them were described by visual observations of loosely defined features, such as cell size, which has led to the description of many duplicate species. In an attempt to fix these issues, Foissner and Wölfl sorted through the many accounts of *Stentor* species, noted likely duplicates, and laid out the key physical features that should be used when visually defining species [36]. Using their guide, I was able to identify a number of wild *Stentor* species from ponds near Woods Hole, MA.

I sampled eight ponds in the Falmouth, MA area and checked them for the presence of *Stentor*. Of those eight, I was able to find *Stentor* in two of the ponds. Over the course of three summers I isolated five species, all of which were present each year. Samples were collected as described in the “Materials and Methods” section. Images of all of the cells displaying various behaviors were collected (Figure 26) and their descriptions and the rationale for their identification are as follows:

**Name:** *Stentor coeruleus*

Location: 41°33'16.4"N 70°36'55.5"W

Macronuclear Morphology: Moniliform

Cortical Pigment: Blue/Green

Length: 600-800  $\mu\text{m}$

Figure 26: Wild isolates of *Stentor*.

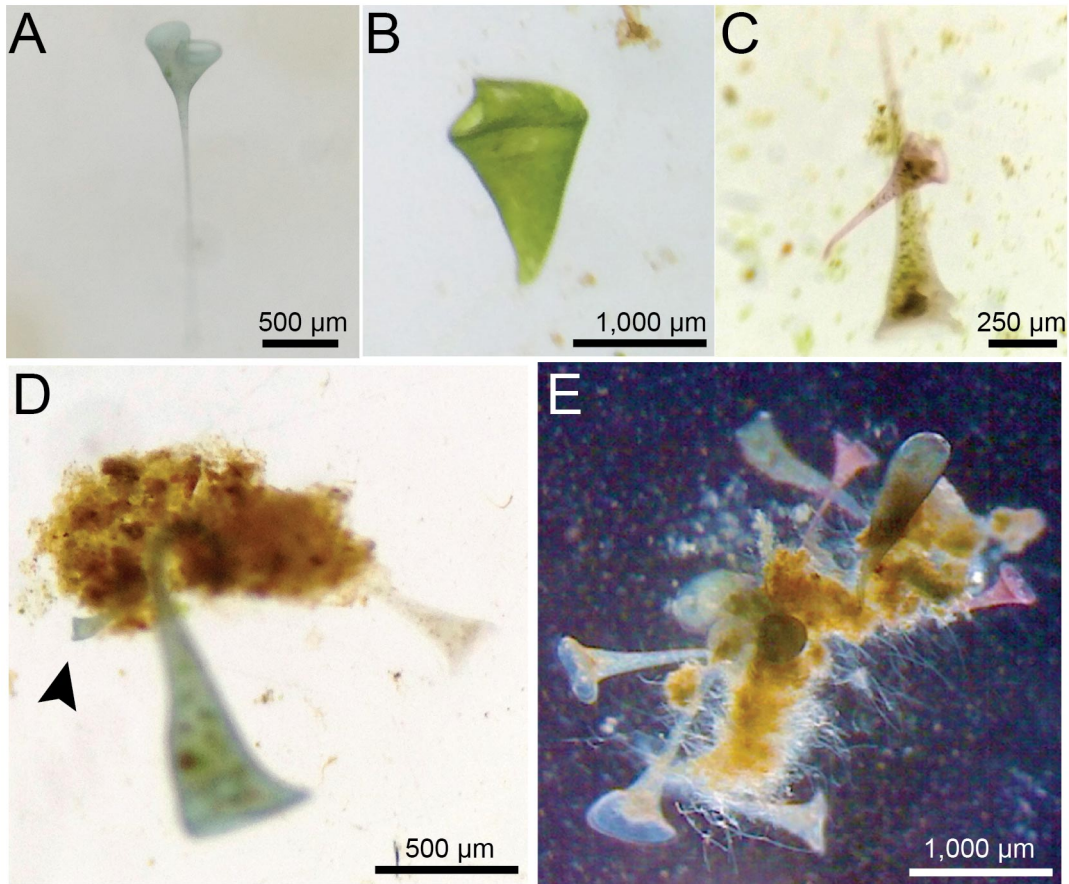


Figure 26. Wild isolates of **(A)** *Stentor coeruleus*. **(B)** *Stentor pyriformis*. **(C)** *Stentor igneus*, which is red, and *Stentor roeselii*, which is unpigmented. **(D)** *Stentor multiformis* (arrow) next to *S. coeruleus* and *S. roeselii* for a direct size comparison. **(E)** Cluster of *S. coeruleus*, *S. roeselii*, and *S. igneus* for direct size comparison. With the exception of *S. pyriformis*, all of these samples were isolated from the same location.

Lorica: None

Endosymbionts: None

Contractility: Highly contractile

Rationale and Details: These cells were extremely rare and I was only able to obtain one or two cells per season. This is likely a result of my sampling methods simply not collecting in the locations that these cells are more abundant. The few cells I did find were always found in and around sediment from the bottom of the pond, which I typically avoided as the opacity made it difficult to find cells. Although I often found cells in the wild that were very mildly pigmented, after a few days of being isolated they became normally pigmented for *S. coeruleus* cells. Additionally, their size, shape, and macronuclear morphology were consistent with *S. coeruleus*. I was able to start a culture from a single cell, and have kept those cells growing for over a year. They are identical to the *S. coeruleus* cells obtained from Carolina Biological Supply, behave identically, regenerate identically, and RNAi vectors yield the same phenotypes (data not shown). From these observations I would conclude that these cells are *Stentor coeruleus*.

**Name: *Stentor roeselii***

Location: 41°33'16.4"N 70°36'55.5"W

Macronuclear Morphology: Vermiform

Cortical Pigment: Colorless

Length: 400 - 600  $\mu\text{m}$

Lorica: Yes, gelatinous

Endosymbionts: None

Contractility: Highly contractile

Rationale and Details: These cells are highly abundant, more so than any of the other species also found at this location using my sampling methods. They are most often found freely swimming around in the pond or attached to vegetation that is floating near the surface of the pond. In their swimming form they typically have a bell shape, with a very round posterior and their anterior with an appearance similar to that of an extended cell. When extended, the cells become extremely long and slender, with the majority of their bodies looking similar to the tail region of *Stentor coeruleus*. Their oral apparatus flares open quite dramatically at the anterior end in stark contrast to their thin body forms. Like *S. coeruleus*, *S. roeselii* also tend to form clusters where many cells will anchor around the same location and the cells fan out with an almost floral appearance (Figure 27A, B). They do this in isolated cultures as well as in the wild, where they normally attach to leaves or other debris (Figure 27C). Cells also build lorica around them when attached, although the structure of their lorica can vary (Figure 27D). Sometimes they are quite organized, almost giving the appearance of multiple rings stacked on top of one another, but often they are much more disorganized and look like large globular chunks of material aggregated near the posterior end of the organism. The reasons for the variability between the two forms of lorica are unknown but I think that it has to do with the environment. Cells taken from a sample housed within organized lorica often were found to make disorganized lorica after isolation, so this is not confusion between two similar looking species. In addition to variability in the constructed lorica, there is also a lot of variability in the cells appearance. The differences between their anchored and swimming forms have already been discussed,

**Figure 27: Features of *Stentor* during growth and division.**

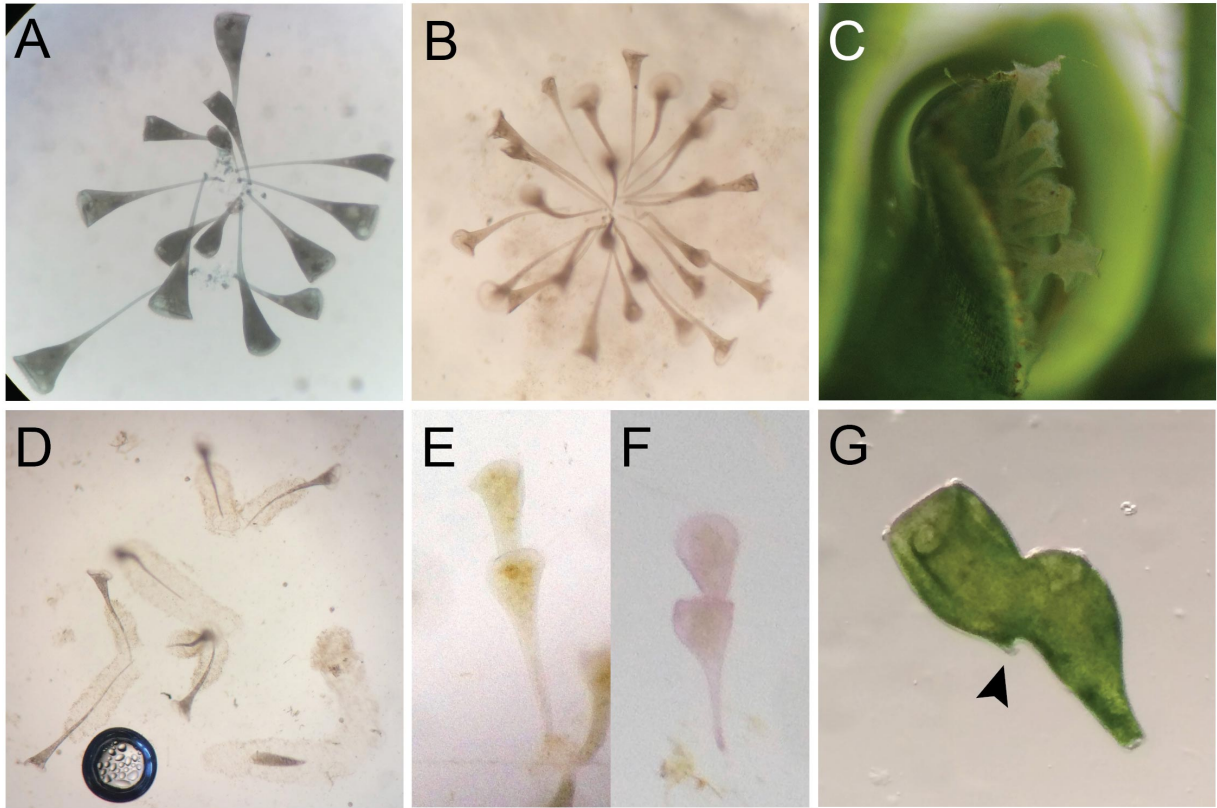


Figure 27. **(A)** Cluster of *S. coeruleus*. **(B)** Cluster of *S. roeselii*. **(C)** Cluster of *S. roeselii* that was obtained directly from the pond, with the leaf still intact **(D)** Organized lorica formed by *S. roeselii*. Cells are able to contract into these for protection (bottom). **(E)** Stage 6 of cell division in *S. roeselii*. **(F)** Stage 6 of cell division in *S. igneus*. **(G)** Stage 6 of cell division in *S. pyriformis*. Although it is slightly different from morphologies seen in other *Stentor* species, the free tail of the anterior daughter can be seen (arrow).

but cells can also appear extremely clear, or slightly darker in appearance with an almost grayish tint. It is unclear whether the pigment difference is actually due to pigments within the cell or some effect of their diet. Due to the variability within this species, numerous names have been given to them. Foissner and Wölfl claim that observations of *S. fimbriatus*, *S. fuscus*, *S. gracilis*, *S. magnus*, *S. roeseli*, *S. stagnalis*, and *S. viridis* are all in fact occurrences of *S. roeselii*. My observations are consistent with those of Foissner and Wölfl.

**Name:** *Stentor igneus*

Location: 41°33'16.4"N 70°36'55.5"W

Macronuclear Morphology: Single Node

Cortical Pigment: Red

Length: 150 - 300  $\mu\text{m}$

Lorica: None

Endosymbionts: None

Contractility: Highly contractile

Rationale and Details: These cells are much smaller than most other *Stentor* species and their MAC is only a single small node. They are, however, the second most abundant species in the pond at this location, although their presence in my samples was much less consistent than *S. roeselii*. Their most obvious feature is the red/pink cortical pigment. Despite their small size, their form looks quite similar to that of *S. coeruleus* and like other *Stentor* species have a very typical morphogenesis during cell division (Figure 27E, F). They have a compact swimming form and the ability to anchor and extend out to nearly 600  $\mu\text{m}$ , with similar proportions to those of *S. coeruleus*.



Foissner mentions two synonymous species, *S. roseus* and *S. ruber*, and all of my observations are consistent with *igneus*.

**Name:** *Stentor multiformis*

Location: 41°33'16.4"N 70°36'55.5"W

Macronuclear Morphology:

Cortical Pigment: Blue/Green

Length: 100-200 μm

Lorica: None

Endosymbionts: None

Contractility: Highly contractile

Rationale and Details: These cells were the smallest *Stentor* cells that I identified (Figure 26D). The pigment looks nearly identical to that of *S. coeruleus* although slightly more vibrant. The defining differences of these cells are that they are much smaller than *S. coeruleus* and also contain a MAC that consists of only a single node. Foissner mentions that *S. multiformis* can often be confused with small members of the *S. coeruleus* species, but I am confident that the cells I found were indeed *S. multiformis* as they never grew larger and multiple MAC nodes were never observed. Like *S. coeruleus*, these cells were isolated very rarely and I only ever saw two of them over the three seasons I sampled.

**Name:** *Stentor pyriformis*

Location: 41°33'27.5"N 70°36'11.0"W

Macronuclear Morphology: Few nodes

Cortical Pigment: None

Length: 750 - 1000  $\mu\text{m}$

Lorica: None

Endosymbionts: Green algal Chlorella

Contractility: Low contractility

Rationale and Details: Unlike all of the other species discussed so far, these cells were found in a different pond and were extremely abundant. Also, their large size, intense green color, and the clarity of the pond allowed me to observe their presence by eye at the pond site. This species was initially difficult to identify, as I first mistook it for *Stentor amethystinus*, which is known to contain green algal endosymbionts. Then, after I discovered that the cells did not contain any purple pigment granules I reclassified the cells as *Stentor fulginiosis*, which is reported to be very similar to *S. amethystinus* but lacks the purple pigment. However, after further investigation I learned that both *S. amethystinus* and *S. fulginiosis* are normally contractile and the cells that I had isolated were only very slightly contractile and just at the extreme posterior end of the cell at the anchor site. Additionally, they had a rather intriguing morphology during division, where the cells would stay attached to one another for much longer than division in other *Stentor* species (Figure 27G). It is interesting to note that the newly forming tail in the anterior daughter can already be seen at early stages of division and does not appear to be at the site of connection between the daughters like in other species (Figure 27G, arrow). Therefore I continued to look for species whose description matched the cells and found *Stentor pyriformis*, which is a synonymous species with *S. oligonucleatus*.

All of these species have been reported in many locations around the globe and are thought to be ubiquitous. Hopefully that is an indication that finding and studying more samples will be easier to do, which I think would be especially interesting. Here it would be important to note that although I have never witnessed conjugation in lab strains of *S. coeruleus*, I was able to witness conjugation in both *S. igneus* and *S. pyriformis* within 48 hours of isolation from the wild (Figure 28). If we could use the genome sequencing efforts in *S. coeruleus* to inform the genome sequencing and assembly of these other species we could then start an effort to identify differences between them. The diversity within the *Stentor* species could lead to fascinating discoveries about the mechanisms that determine cell size or shape and these species could potentially be interesting case studies of endosymbiosis. It would be especially useful if tools developed in *S. coeruleus* could be applied to other isolated species.

**Figure 28: Conjugation in wild *Stentor*.**

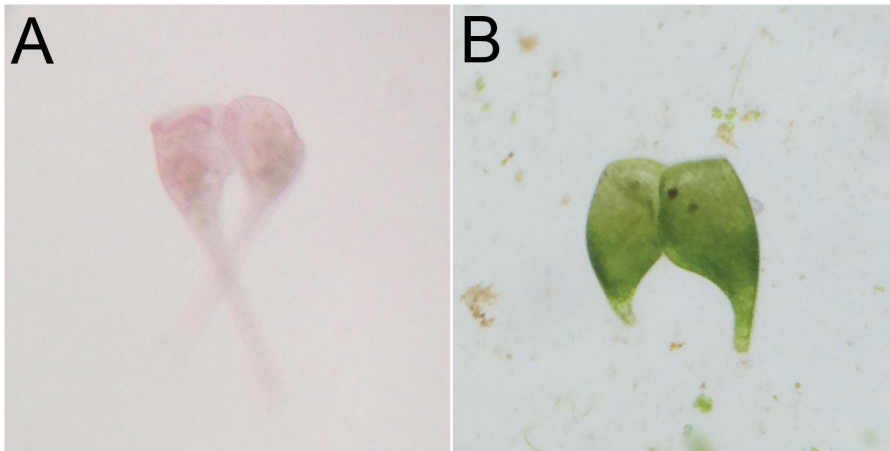


Figure 28. Conjugation was seen between 24 and 48 hours after isolation into fresh media in two different *Stentor* species, *igeneus* (A) and *pyriformis* (B). Both were observed after mating pairs had already been formed and the pairs lasted for 3-6 hours after observation began. The entire length of conjugation cannot be determined from my observations.

## Chapter 6: Materials and Methods

### *Culturing and Media*

*Stentor coeruleus* cells were obtained commercially (Carolina Biological Supply, Burlington, NC) but subsequently maintained in culture within the lab by growing in the dark at 20°C in Modified *Stentor* Medium (MSM), 0.75 mM Na<sub>2</sub>CO<sub>3</sub>, 0.15 mM KHCO<sub>3</sub>, 0.15 mM NaNO<sub>3</sub>, 0.15 mM KH<sub>2</sub>PO<sub>4</sub>, 0.15 mM MgSO<sub>4</sub>, 0.5 mM CaCl<sub>2</sub>, 1.47 mM NaCl modified from the original recipes described by Tartar [2] and De Terra [37]. This medium provides no nutrients and must be supplemented with living prey. In order to provide prey with a known genome, we use *Chlamydomonas reinhardtii* grown separately in TAP medium[38] and washed in MSM before feeding. 300mL *Stentor* cultures are given  $3 \times 10^7$  *Chlamydomonas* cells two or three times per week.

### *Cloning of Stentor gene sequences*

Homologs were identified by best-reciprocal BLAST starting with *Paramecium tetraurelia* proteins (Table 1). Target gene sequences were obtained by PCR amplification from genomic DNA and cloned into pPR-T4P (kind gift from J. Rink), a modified pDONR-dT7 in which a ligation-independent cloning site was added [39]. Cloning was performed by either the ligation-independent method or by cohesive-end ligation. Additional information about the RNAi constructs used in this study is included in a supplemental table (Table 3).

**Table 3: Details about RNAi vectors used.**

Construct name	Target gene	Length (bp)	Relative positions within coding region	Forward primer	Reverse primer
pPR-Sciw03	Sciw03	1203	844-2045	TAGTCCCAGAATTTGTGTTATGACAGG	CCATTTTCTCAACAACCGTCTAGACG
pPR-Atub	ATU02	1147	94-1236	TCAACCTGACGGTCAAATGCCTTC	ACCTTCACCGACATACCAGTGAACG
pPR-Btub_1-1333	BTU05	1332	1-1332	ATGAGAGAAATTGTTACGTACAAGGC	TTAAGCAGCTTCCTCTTCTCATCG
pPR-Btub	BTU05	659	1-659	ATGAGAGAAATTGTTACGTACAAGGC	GGAGTAGTGAGCTTAAGAGTTCTGAAGC
pPR-Btub	BTU05	668	665-1332	ATGGTGACTTAAATCACTTGGTTAGTGC	TTAAGCAGCTTCCTCTTCTCATCG
pPR-LF4	LF4a	876	8-884	CAGAATACCGTTTGATATCAAAAAAAGGTGAAGG	CTACTTGCCTCATCAACAAAATCTTTGAAATAAGG
pPR-Mob1	Mob1a	633	40-672	AAGAAGCGAATTGAAAAAGGCCAGC	GTTACCAGAAGCTTCTCTTCCATTCTTCC
pPR-Mob1_40-356	Mob1a	317	40-356	AAGAAGCGAATTGAAAAAGGCCAGC	CAGGTCATGAGAAAATCAATATACTCTGATGC
pPR-Mob1_326-672	Mob1a	347	326-672	CATCAGAGTATATTGATTTCTCATGACCTGGG	GTTACCAGAAGCTTCTCTTCCATTCTTCC

Table 3. Summary of all RNAi constructs used in this experiment, their lengths and relative positions within the coding sequence, and primers used to amplify the sequences from genomic samples.

### *Phylogenetic Analysis*

Multiple sequence alignments were made using ClustalW2 with default settings. The list of Argonaute proteins used in the analysis is included in a supplemental table (Table S2). The un-rooted neighbor-joining tree was made with 1,000 bootstrap replicates using the MEGA v5.1 program [40]. FigTree v1.4 was used to visualize the tree data.

### *RNA Interference*

RNAi was performed by transforming HT115 *E. coli* with each plasmid to allow for dsRNA expression of the target gene. Transformed bacteria were grown to log phase and then induced with 1mM IPTG for 3 hours at 37°C. After induction, bacteria were washed and resuspended in MSM then fed to *Stentor* that had been previously starved for 24-48 hours. Induction and feeding of bacteria was then repeated for 2-5 days. Negative controls used for RNAi experiments were either pPR-Sciwi03 or pPR-LF4.

### *Quantitative PCR Assay*

RNA was extracted from 50 cells per sample using PureLink RNA mini kit (Life Technologies, Grand Island, NY). After purification RNA was treated with DNaseI (New England Biolabs, Ipswich, MA), repurified, and then primed with oligo-dT and reverse transcribed using the SuperScript III kit (Life Technologies, Grand Island, NY). Samples were diluted as necessary and 5  $\mu$ L were used in each qRT-PCR reaction. Reactions were run on a C1000 ThermoCycler (Bio-Rad, Hercules, CA) with an annealing temperature of 54°C. Primer sets were designed for  $\alpha$ - and  $\beta$ - tubulin, GAPDH, and

Mob1 (Table S4). Each qRT-PCR run was finished with a melt curve to determine the homogeneity of the amplified product. Starting quantity was calculated using a standard curve and a genomic DNA control for each primer pair. 3 technical replicates were performed for each of 1-3 biological replicates. Error bars represent standard deviation for biological replicates. For samples with 1 biological replicate, standard deviation of technical replicates is shown with uncapped error bars.

### *Antibodies*

Mouse monoclonal anti-acetylated tubulin (clone 6-11B-1) was used at a 1:500 dilution (Sigma, St. Louis, MO). MOB1 antibody was generated in rabbits whose pre-immune bleeds had been screened before immunization using the synthetic peptide N-CFIDRFKLVDQKELAPLAELI-C (Covance, Denver, PA) and affinity purified using a SulfoLink Immobilization Kit for Peptides (Pierce Biotechnology, Rockford, IL). Purified Mob1 antibody was used at a concentration of 3  $\mu\text{g}/\text{mL}$ . Alexa-488 goat-anti-mouse and Alexa-488 goat-anti-rabbit secondary antibodies (Life Technologies, Grand Island, NY) were used for immunofluorescence and IRDye 800CW goat-anti-mouse and IRDye 680RD goat-anti-rabbit secondary antibodies (LI-COR Biosciences, Lincoln, NE) were used for Western blotting.

### *Immunofluorescence*

Cells were isolated from culture and washed in fresh MSM. Cells were then isolated in minimal volume in a 1.5 mL tube for fixation and staining in suspension. Cells were fixed



**Table 4: Primers used for cloning.**

Primer Name	Primer Sequence
MOB1_Forward	AGAGTTTCAGGCCGAAGAAGAG
MOB1_Reverse	CGTTCAAGTCTTCACCTGTTGG
GAPDH_Forward	AACGGGTTTGGGAGAATAGGTC
GAPDH_Reverse	CCTGGGTAATTTCCATGGACTG
Alpha-Tubulin_Forward	TTTGTTGACTGGTGCCCAAC
Alpha-Tubulin_Reverse	AGCAATGGCAGTTGAGTTGC
Beta-Tubulin_Forward	ACATTCTCTTGGTGGTGGTACC
Beta-Tubulin_Reverse	TGTCTGAGACCTTTGGTGATGG

Table 4. Oligonucleotide sequences used for the qRT-PCR analysis of *Stentor* genes.

in ice-cold methanol for 10 minutes at -20°C, rehydrated at room temperature in a 1:1 MeOH:PBS mixture for 5 minutes, and 1x PBS for 10 minutes. Cells were blocked in 1x PBS, 2% BSA, and 0.1% Triton-X-100 for 1 hour at room temperature. In order to avoid centrifugation, cells were allowed to settle to the bottom of the tube between steps.

#### *Immunoprecipitation / Western Blotting*

1,500 *Stentor* cells were washed 3x in MSM, 1x in ice cold MSM and lysed in 50mM Tris-HCl pH 8.0, 125 mM NaCl, 1% NP-40 containing a complete protease inhibitor cocktail tablets (Roche Diagnostics Corp., Indianapolis, IN), mixed by pipetting and incubated for 30 minutes while rotating at 4°C. Lysates were centrifuged at 10,000 xg for 15 minutes at 4°C and the supernatant was incubated with anti-Mob1 antibody for 2 hours while mixing at 4°C. Samples were then incubated with Protein A Anti-Rabbit IgG beads overnight while mixing at 4°C (Rockland Immunochemicals Inc., Boyertown, PA). Sample buffer was added and boiled for 10 minutes before running on a 10% SDS-PAGE gel and transferred onto a nitrocellulose membrane. Blots were probed with anti-Mob1 primary antibody (1:500) and Rabbit IgG TrueBlot secondary antibody (1:1000) (Rockland Immunochemicals Inc., Boyertown, PA), developed using Chemiluminescent HRP substrate, and exposed to film.

#### *Imaging*

Brightfield images were collected on a Stemi 2000C and an Axio Zoom V16 equipped with a 1x and 2.3x objective (Carl Zeiss MicroImaging, Thornwood, NY). Images were captured using an AxioCam MRc digital microscope camera (Carl Zeiss MicroImaging,

Thornwood, NY) or a Rebel T3i digital SLR camera (Canon U.S.A., Inc., Melville, NY). DIC images were captured on an Axiovert 200M microscope (Carl Zeiss MicroImaging, Thornwood, NY) equipped with 10x 0.22 NA and 40x 0.75 NA objectives with an AxioCam MRm digital microscope camera (Carl Zeiss MicroImaging, Thornwood, NY). Fluorescence images were collected on Deltavision deconvolution microscope (Applied Precision, Issaquah, WA) equipped with 10x 0.4 NA, 20x 0.5 NA, and 100x oil 1.4NA objectives using a CoolSnap HQ (Photometrics, Tuscon, AZ) digital microscope camera. Immunofluorescence images are Z-stacks taken with 2  $\mu\text{m}$  step sizes for 20x images and 0.2  $\mu\text{m}$  step sizes for 100x images. Images of cells that were too large to fit into a single image were manually stitched using the cortical rows to align the two images and the seam is indicated with yellow dashed lines.

### *Cell Shape Analysis*

Brightfield images of live, fully extended cells were first binarized using ImageJ v1.46. A custom MATLAB program was then used to create an outline and midline of the binarized cell image (Figure 9, code available upon request). Perpendicular lines were computed every 10 pixels along the length of the midline and their intersections with the cell outline calculated to define the cell width. Cell lengths were then normalized, and cell width versus cell length was plotted for all cells. The plot shown is a trendline of data from all cells, with a sliding average of  $2n$  the number of samples collected.

In order to compare cell shapes between control and RNAi cells using this analysis, we define a shape factor that summarizes the shape of each cell as follows: for each cell,

the widest point of the cell outline is assumed to represent the OA while the point furthest away from the OA is assumed to represent the tail. The area of the cell contained between those two extremes is then calculated by numerical integration using the trapezoidal rule. For comparison, the area of the right trapezoid constructed by drawing a straight line from the tail point to the OA outline point. We then define the shape factor as the ratio of the actual area to the area of the right trapezoid. This unitless parameter will have a value of 1 if the cell is a perfect right cone, i.e. if its sides are perfectly straight (a cylinder would be a special case of this). Thus, the more conical or cylindrical the cell is, the closer the shape factor gets to 1. If the cell has a taper like a wine glass or a wile-type *Stentor* cell, it will have a shape factor of less than 1. The change in cell shape from tapering to cylindrical seen in Mob1 RNAi is thus reflected by an increase in shape factor.

### *Microsurgery*

Surgery was performed following methods reported by Tartar [13]. Cells were isolated from culture and washed in fresh MSM. Cells were transferred to 1-2% Methylcellulose (Sigma, St. Louis, MO) in MSM, mounted on a slide in a 1 cm x 1 cm well, and visualized on a Olympus Stemi-2000c stereoscope. Microsurgery was performed using glass-stirring rods (Fisher, Pittsburgh, PA) after hand pulling glass needles from the tips of the rods using a butane torch or Bunsen burner.

### *Isolation of gDNA*

300 cells were washed 3x in fresh MSM and incubated without additional food for 48 hours. After starvation, cells were again washed 3x in MSM and isolated in minimal media. Genomic DNA was isolated using the DNeasy Blood and Tissue kit (Qiagen), following the suspension cell protocol, and eluting in 75  $\mu$ L yielding 3 $\mu$ g. Whole cell DNA was isolated, and thus should contain DNA from both the macronucleus as well as the micronucleus, but we believe this isn't an issue for two reasons. First, when inspected by DAPI staining there are no micronuclei visible in our Carolina strains and so they may be amiconucleate. Secondly, if there are micronuclei present, the DNA content of the macronucleus represents the vast majority of the nuclear content and so micronuclear contamination would be an extremely small percentage of the sequenced DNA and could be identified and filtered by coverage. Samples were checked for *Chlamydomonas* contamination using PCR amplification of the mating type locus, but no contamination was detected.

#### *ddPCR and ploidy measurements*

Single cell DNA samples were prepared and 2  $\mu$ L of the sample were used as the DNA template in the ddPCR reaction. Dual labeled probes were ordered with either 5'-FAM or 5'-HEX as the fluorescent indicator and ZEN-Iowa Black quenchers (Integrated DNA Technologies, Inc., Coralville, IA). ddPCR reactions were prepared using the 2x ddPCR Supermix (Bio-Rad) with target amplification primers (900 nM) and probes (500 nM) on the QX100 ddPCR system (Bio-Rad). Droplet generation, PCR, and droplet detection were performed following the QX100 system protocols (Bio-Rad). Briefly, 25  $\mu$ L PCR samples were loaded onto 8-well cartridges with 65  $\mu$ L of droplet generation oil and

placed on the droplet generator (Bio-Rad). Droplets were then loaded onto 96-well PCR plates, heat-sealed, and PCR was performed on a standard thermal cycler. Plates were then transferred to the QX100 droplet reader (Bio-Rad) and analysis was performed using QuantaSoft (Bio-Rad). In order to determine the ploidy of a single cell, the “copies-per-microliter” value was multiplied by 250 to account for both the 25  $\mu$ L PCR volume and initial sample volume of 20  $\mu$ L.

Target	Forward Primer	Reverse Primer	Probe
Contig_2	AAAGATGGCCAAGTGCAAAG	TCGTTCTAATCCTGCCATATCC	AGTCCAGATCCTACAATTGGAGTATGT
Contig_18	TGTACTGCTCAAAGGTACACTAAG	CATTGATGCAGCTTGAAGATAAGG	CACCTTCAGACGATTGCTCATTATTGC
Contig_43	ACCTTCTTCCACATCACAATCT	AGAGATCATGGGAGGTTATAGGA	ACCCATCATCCAACATCCTCCTCTCT
Contig_558	CCTACTCGGCCCATCAAATC	TCAGAAGCTAGCTCAGGATACA	TGCACAGACCAAATCCCATTGTCTCT
Contig_2227	CCTACCGATTTCGAGTGATGAG	CCTTGTTACGACTTCTCCTTCC	TACTCAACTCCCAACGCCGAAGC
pPR-T4P Plasmid	CTACATACCTCGCTCTGCTAATC	GCGCCTTATCCGGTAACTATC	AAGACACGACTTATCGCCACTGGC

### *Isolation of Stentor from fresh water lakes and ponds*

Different species of *Stentor* have different behaviors, and thus the specific methods for sampling will likely influence the types of species that are found. For my studies, I waded into fresh water ponds in Falmouth, MA and looked for shaded areas of the pond that also contained a lot of vegetation growing out of the water, or floating on the surface. I used a wide-mouthed container, such as a 500 mL beaker or 2 cup measuring cup to scoop up water containing leaves or other vegetation that *Stentor* might be attached to. Samples were then agitated by stirring or shaking (if the container had a lid) for about a minute before pouring the liquid into sample containers that were sealed for transport. After returning to the lab I would then pour out the samples into petri dishes and manually search through the pond samples ~50 mL at a time looking for anything

that appeared to be *Stentor*. I would isolate any identified cells and transfer them into a culture dish for verification and observation.

## Chapter 7: Bibliography

1. Trembley, A. (1744). Translation of a Letter from Mr. Abraham Trembley, F. R. S. to the President, with Observations upon Several Newly Discover'd Species of Fresh-Water Polypi. *Philosophical Transactions of the Royal Society of London* 43, 169–183.
2. Tartar, V. (1961). *The Biology of Stentor* (Pergamon Press).
3. Song, P.-S., H der, D.-P., and Poff, K. L. (1980). Step-up photophobic response in the ciliate, *Stentor coeruleus*. *Arch. Microbiol.* 126, 181–186.
4. Huang, B., and Pitelka, D. (1973). The contractile process in the ciliate, *Stentor coeruleus*. *The Journal of Cell Biology* 57, 704–728.
5. Miyake, A., Harumoto, T., and Iio, H. (2001). Defence function of pigment granules in *Stentor coeruleus*. *European Journal of Protistology* 37, 77–88.
6. Dai, R., Yamazaki, T., Yamazaki, I., and Song, P. (1995). Initial spectroscopic characterization of the ciliate photoreceptor stentorin. *Biochimica et Biophysica Acta (BBA)-Bioenergetics* 1231, 58–68.
7. Wood, D. C. (1969). Parametric studies of the response decrement produced by mechanical stimuli in the protozoan, *Stentor coeruleus*. *J. Neurobiol.* 1, 345–360.
8. Wood, D. C. (1988). Habituation in *Stentor*: produced by mechanoreceptor channel modification. *The Journal of neuroscience*.
9. Morgan, T. (1901). Regeneration of proportionate structures in *Stentor*. *The*



- Biological Bulletin 2, 311.
10. Kirschner, M., Gerhart, J., and Mitchison, T. (2000). Molecular “Vitalism” Review. *Cell* 100, 79–88.
  11. Shulman, J., and St Johnston, D. (1999). Pattern formation in single cells. *Trends in Genetics* 15, M60–M64.
  12. Tartar, V. (1960). Reconstitution of minced *Stentor coeruleus*. *Journal of Experimental Zoology* 144, 187–207.
  13. Tartar, V. (1956). Grafting experiments concerning primordium formation in *Stentor coeruleus*. *Journal of Experimental Zoology* 131, 75–121.
  14. Tartar, V. (1957). Reactions of *Stentor coeruleus* to certain substances added to the medium. *Experimental Cell Research* 13, 317–332.
  15. Tartar, V. (1953). Chimeras and nuclear transplantations in ciliates, *stentor coeruleus* X *S. polymorphus*. *Journal of Experimental Zoology* 124, 63–103.
  16. De Terra, N. (1985). Cytoskeletal discontinuities in the cell body cortex initiate basal body assembly and oral development in the ciliate *Stentor*. *Journal of embryology and experimental morphology* 87, 249.
  17. Weisz, P. (1951). An experimental analysis of morphogenesis in *Stentor coeruleus*. *Journal of Experimental Zoology* 116, 231–257.
  18. Luca, F. C., and Winey, M. (1998). MOB1, an essential yeast gene required for completion of mitosis and maintenance of ploidy. *Mol Biol Cell* 9, 29–46. Available

at: <http://www.molbiolcell.org/content/9/1/29.short>.

19. Nelson, B., Kurischko, C., Horecka, J., Mody, M., Nair, P., Pratt, L., Zougman, A., McBroom, L. D. B., Hughes, T. R., Boone, C., et al. (2003). RAM: a conserved signaling network that regulates Ace2p transcriptional activity and polarized morphogenesis. *Mol Biol Cell* *14*, 3782–3803.
20. Lai, Z.-C., Wei, X., Shimizu, T., Ramos, E., Rohrbaugh, M., Nikolaidis, N., Ho, L.-L., and Li, Y. (2005). Control of cell proliferation and apoptosis by mob as tumor suppressor, mats. *Cell* *120*, 675–685.
21. Hergovich, A. (2011). MOB control: reviewing a conserved family of kinase regulators. *Cellular signalling* *23*, 1433–1440.
22. Tavares, A., Gonçalves, J., Florindo, C., Tavares, A. A., and Soares, H. (2012). Mob1: defining cell polarity for proper cell division. *J Cell Sci* *125*, 516–527.
23. Ruby, J. G., Bellare, P., and Derisi, J. L. (2013). PRICE: Software for the Targeted Assembly of Components of (Meta)Genomic Sequence Data. *G3 (Bethesda)* *3*, 865–880.
24. Bouhouche, K., Gout, J.-F., Kapusta, A., Bétermier, M., and Meyer, E. (2011). Functional specialization of Piwi proteins in *Paramecium tetraurelia* from post-transcriptional gene silencing to genome remodelling. *Nucleic Acids Res* *39*, 4249–4264.
25. Rivas, F. V., Tolia, N. H., Song, J.-J., Aragon, J. P., Liu, J., Hannon, G. J., and

- Joshua-Tor, L. (2005). Purified Argonaute2 and an siRNA form recombinant human RISC. *Nat. Struct. Mol. Biol.* *12*, 340–349.
26. Galvani, A., and Sperling, L. (2002). RNA interference by feeding in *Paramecium*. *Trends Genet* *18*, 11–12.
  27. Sobierajska, K., Joachimiak, E., Bregier, C., Fabczak, S., and Fabczak, H. (2011). Effect of phosducin silencing on the photokinetic motile response of *Blepharisma japonicum*. *Photochem. Photobiol. Sci.* *10*, 19–24.
  28. Paulin, J., and Brooks, A. (1975). Macronuclear differentiation during oral regeneration in *Stentor coeruleus*. *J Cell Sci* *19*, 531.
  29. Asleson, C. M., and Lefebvre, P. A. (1998). Genetic analysis of flagellar length control in *Chlamydomonas reinhardtii*: a new long-flagella locus and extragenic suppressor mutations. *Genetics* *148*, 693–702.
  30. Berman, S. A., Wilson, N. F., Haas, N. A., and Lefebvre, P. A. (2003). A novel MAP kinase regulates flagellar length in *Chlamydomonas*. *CURBIO* *13*, 1145–1149.
  31. Citterio, S., Piatti, S., Albertini, E., Aina, R., Varotto, S., and Barcaccia, G. (2006). Alfalfa Mob1-like proteins are involved in cell proliferation and are localized in the cell division plane during cytokinesis. *Experimental Cell Research* *312*, 1050–1064.
  32. Luca, F. C., Mody, M., Kurischko, C., Roof, D. M., Giddings, T. H., and Winey, M.

- (2001). *Saccharomyces cerevisiae* Mob1p is required for cytokinesis and mitotic exit. *Mol Cell Biol* 21, 6972–6983.
33. Ovchinnikova, L. P., Cheissin, E. M., and Selivanova, G. V. (1965). Photometric study of the DNA content in the nuclei of *Spirostomum ambiguum* (Ciliata, Heterotricha). *Acta Protozoologica* 3, 69–78.
  34. De Terra, N. (1967). Macronuclear DNA synthesis in *Stentor*: regulation by a cytoplasmic initiator. *Proceedings of the National Academy of Sciences of the United States of America* 57, 607.
  35. Preer, L. B., Rudman, B., Pollack, S., and Preer, J. R. (1999). Does ribosomal DNA get out of the micronuclear chromosome in *Paramecium tetraurelia* by means of a rolling circle? *Mol Cell Biol* 19, 7792–7800.
  36. Foissner, W., and Wöfl, S. (1994). Revision of the genus *Stentor* Oken (Protozoa, Ciliophora) and description of *S. araucanus* nov. spec, from South American lakes. *Journal of plankton research* 16, 255.
  37. De Terra, N. (1966). Culture of *Stentor coeruleus* on *Colpidium campylum*. *J Eukaryotic Microbiology* 13, 491–492.
  38. Harris, E. H. (2009). *The Chlamydomonas Sourcebook*, Volume 1.
  39. Aslanidis, C., and de Jong, P. J. (1990). Ligation-independent cloning of PCR products (LIC-PCR). *Nucleic Acids Res* 18, 6069–6074.
  40. Tamura, K., Peterson, D., Peterson, N., Stecher, G., Nei, M., and Kumar, S.

(2011). MEGA5: Molecular Evolutionary Genetics Analysis Using Maximum Likelihood, Evolutionary Distance, and Maximum Parsimony Methods. *Molecular Biology and Evolution*.

## Appendix: **Quick Guide: *Stentor coeruleus***

### ***What is Stentor coeruleus?***

*Stentor coeruleus* is an astoundingly large (~1 mm long) single celled pond organism with a distinct trumpet shape and a well-defined morphology (Figure 1). The name stentor is a reference to its trumpet shape and the herald in Greek mythology known for having a loud voice, while coeruleus describes the blue-green pigment specific to the species. Abraham Trembley, who thought it was a type of hydra, first identified *Stentor* in 1744; but actually *Stentor* is a member of the Ciliate phylum in the class Heterotrichae.

*Stentor* isn't just big and blue. It has a highly complex body plan and a rich repertoire of behaviors, including the ability to learn. But *Stentor* is most famous for its amazing regenerative abilities. If a *Stentor* cell is cut in half, each half regenerates a half-sized cell with normal anatomy. Even if a single cell is cut into multiple small fragments, each fragment will generate into a normal-looking cell. The fact that a single cell could rebuild its complex anatomy while displaying many of the same developmental processes as animal embryos, including axiation and induction, grabbed the attention of the leading embryologists around 1900, including Balbiani, F. R. Lillie, and even Thomas Hunt Morgan. Following the lead of these early luminaries, Vance Tartar and Noël De Terra developed an astounding variety of microsurgical procedures designed to probe the mechanism of regeneration. Perhaps the most interesting classical discovery is that *Stentor* cells possess a region of their cortex known as the locus of stripe contrast, where widely spaced cortical rows are adjacent to narrowly spaced rows, which can induce the formation of additional body axes similar to an

organizer region in metazoan development. But despite the challenges that these surgical observations raise for basic cell biology, *Stentor* was never developed as a molecular model system until now, and the mechanism of pattern formation and regeneration in *Stentor* remains unknown.

### ***How can fragments of a single celled organism regenerate into whole organisms?***

One of the most fascinating unanswered questions about *Stentor* is how the cell is able to heal and regenerate after injury. Why doesn't the cytoplasm leak out after the cell is cut open? How are multiple cells able to regenerate from different fragments of an original cell? How does a cell know which structures are missing and then specifically and properly regenerate them? There must be molecular pathways that determine which structures are present, and which are missing and thus need to be replaced, but how this works is a complete mystery that challenges our fundamental conception of what a cell can and can't do.

### ***What are the limitations to regeneration?***

Almost any piece of *Stentor* can regenerate as long as it contains part of the macronucleus and a small portion of the original cell membrane/cortex. The macronucleus in *Stentor* is highly polyploid and extends along the length of the whole cell. Due to the high ploidy, even a fraction of the macronucleus will contain many copies of the entire genome, which is one of the reasons this cell can regenerate after being cut into small pieces. As for the quantity of cytoplasm needed to support regeneration, Lillie and Weisz both found that surgically produced cell fragments must

be at least 70-80  $\mu\text{m}$  in diameter in order to regenerate given the presence of a macronuclear node. Also, grafting multiple cells together is possible and in some cases the two cells can maintain a fused state and divide as a stable doublet cell with two mouths and a single tail in the proper orientation. These experiments highlight the phenomenon of cortical inheritance often seen in ciliates, and has been well studied by Joseph Frankel in *Tetrahymena thermophila*.

### ***Why isn't Stentor more widely studied?***

Although *Stentor coeruleus* was quite well studied through the mid-1900s, the inability to grow cells at high densities and the inability to perform genetic crosses due to low mating frequencies likely persuaded scientists to turn to better biochemical and genetic models for study. In addition, the vast majority of the microsurgical work was performed by just two scientists, Vance Tartar and Noël De Terra, both of whom unfortunately passed away before the development of many technologies that have made *Stentor* a more tractable system, and much of their expertise was lost with them.

### ***What can we learn from studying Stentor?***

*Stentor coeruleus* is a great model for studying complex morphogenesis at the level of a single cell without needing to worry about external influences from neighboring cells that are present in metazoan development. Whether or not any of the mechanisms that regulate *Stentor* morphogenesis are conserved in metazoans remains an open question but further research might shed light on how complex single-cells are organized. *Stentor* may also be useful for studying wound healing within cells, as it has



the ability to maintain its integrity even after severe surgical manipulations. As a final example, *Stentor* could be useful as a model for memory at the level of a single cell. Work from David Wood has shown that *Stentor* possesses the ability to habituate to mechanical stimuli and can remain habituated over the course of hours, although no molecular mechanism for this phenomenon has been determined.

### ***What tools are available for studying Stentor?***

*Stentor coeruleus* is easily imaged on even the most basic microscopes at low magnification, where the majority of the cell structures can be resolved. As discussed previously, *Stentor* is amenable to microsurgical manipulation, including surgical removal of specific regions of the cell and even grafting of cell fragments onto other cells. Recently, RNA interference methodology has been adapted and shown to be an effective method for probing gene function in *Stentor*. This can be achieved by feeding the *Stentor* with bacteria expressing long double-stranded RNA corresponding to a gene of interest for 3-5 days.

### ***Do Stentor mate?***

Mating in ciliates is very well studied in systems like *Tetrahymena* and *Paramecium*, but information about conjugation in *Stentor* is currently lacking. There are a handful of studies that describe mating in *Stentor coeruleus*, and show that isolates from different locations have the ability to form mating pairs that look similar to mating pairs from other ciliates. Previous studies on *Stentor*, and work from other ciliates, suggest that stressful conditions such as starvation or temperature shifts can induce

conjugation but we have not found these protocols to be successful in our lab strain. We have seen cells with altered morphologies consistent with descriptions of pre-conjugation but mating pairs have never been obtained. It is therefore possible that our lab strain lacks a micronucleus or that we have cells of only a single mating type. Interestingly, mating pairs have been seen in two different species of *Stentor* obtained from the wild after being isolated for 24-48 hours without additional food, so there is potential for conjugation in *Stentor coeruleus* by isolating cells from natural sources. Development of classical genetics in *Stentor* could be a very powerful tool for furthering *Stentor coeruleus* as a useful model organism.

### ***Is there a Stentor coeruleus genome project?***

The macronuclear genome of *Stentor coeruleus* has been sequenced and assembled, and is currently being annotated in our lab. Once completed, the genome will be publicly accessible on the [stentor.ciliate.org](http://stentor.ciliate.org) server.

### ***Where can I find out more?***

Lillie, FR. (1896) *On the smallest parts of Stentor capable of regeneration*. J. Morphol.

12, 239-249

Morgan, TH. (1901) *Regeneration of proportionate structures in Stentor*. The Biological Bulletin

Tartar, V. (1961) *The Biology of Stentor*. International Series of Monographs on Pure and Applied Biology. 5, 1-434 Pergamon Press

De Terra, N. (1985) *Cytoskeletal discontinuities in the cell body cortex initiate basal body assembly and oral development in the ciliate Stentor*. J. Embryol. Exp. Morph., 87, 249-257

Frankel, J. (2008) *What do genic mutations tell us about the structural patterning of complex single-celled organism?* Euk. Cell 7(10), 1617-1639

Genome Database Wiki: [stentor.ciliate.org](http://stentor.ciliate.org)

Burchill, B.R. (1967) *Conjugation in Stentor coeruleus*. J. Protozool. 14(4), 683-687

Webb, TL. and Francis, D. (1969) *Mating types in Stentor coeruleus*. J. Protozool. 16(4), 758-763

Slabodnick et. al., (2013) *Visualizing cytoplasmic flow during single-cell wound healing in Stentor coeruleus*. JoVE (82) e50848

Slabodnick et. al., (2014) *The kinase regulator Mob1 acts as a patterning protein during Stentor morphogenesis*. PLoS Biology 12(5) e1001861

Wood, DC. (1969) *Parametric studies of the response decrement produced by mechanical stimuli in the protozoan, Stentor coeruleus*. J. Neurobiology 1(3), 345-360

Frankel and Whitely, (1993) *Vance Tartar: A Unique Biologist*. J. Euk. Microbiol. 40(1), 1-9

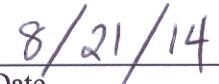
**Publishing Agreement**

*It is the policy of the University to encourage the distribution of all theses, dissertations, and manuscripts. Copies of all UCSF theses, dissertations, and manuscripts will be routed to the library via the Graduate Division. The library will make all theses, dissertations, and manuscripts accessible to the public and will preserve these to the best of their abilities, in perpetuity.*

***Please sign the following statement:***

*I hereby grant permission to the Graduate Division of the University of California, San Francisco to release copies of my thesis, dissertation, or manuscript to the Campus Library to provide access and preservation, in whole or in part, in perpetuity.*

  
\_\_\_\_\_  
Author Signature

  
\_\_\_\_\_  
Date